The Meteoritical Society

Meteoritics & Planetary Science 1–29 (2026)
doi: 10.1111/maps.70232

The Dingle Dell (L6) meteorite fall: In-depth characterization of an L chondrite with some LL-like properties originating from the inner main belt

Seamus L. ANDERSON[1,2]*, Gretchen K. BENEDIX[1,3], Lucy V. FORMAN[1], Luke DALY[4,5,6], Belinda GODEL[7], Lionel ESTEBAN[7], Matthias M.M. MEIER[8], Colin MADEN[9], Henner BUSEMANN[9], Qing-Zhu YIN[10], Matthew E. SANBORN[10], Karen ZIEGLER[11], Jon M. FRIEDRICH[12,13], Kees C. WELTEN[14], Marc W. CAFFEE[15,16], Kieren T. HOWARD[17], Hannah MCLAIN[2,18,19], Katarina YOCUM[2,20], Daniel P. GLAVIN[2], Jason P. DWORKIN[2], Robert MACKE[21], Ashley F. ROGERS[1], Hadrien A.R. DEVILLEPOIX[1,22], Phil A. BLAND[1], Martin C. TOWNER[1], Eleanor K. SANSOM[1,22], and Alex W.R. BEVAN[3]

[1]Space Science and Technology Centre, School of Earth and Planetary Sciences, Curtin University, Perth, Western Australia, Australia
[2]Solar System Exploration Division, Code 690, NASA Goddard Space Flight Center, Greenbelt, Maryland, USA
[3]Department of Earth and Planetary Sciences, Western Australia Museum, Welshpool, Western Australia, Australia
[4]School of Geographical and Earth Sciences, University of Glasgow, Glasgow, UK
[5]Centre for Microscopy and Microanalysis, University of Sydney, Sydney, New South Wales, Australia
[6]Department of Materials, University of Oxford, Oxford, UK
[7]CSIRO, Australian Resources Research Centre, Kensington, Western Australia, Australia
[8]Naturmuseum St. Gallen, St. Gallen, Switzerland
[9]Institute of Geochemistry and Petrology, ETH Zurich, Zurich, Switzerland
[10]Department of Earth and Planetary Sciences, University of California, Davis, Davis, California, USA
[11]Institute of Meteoritics, Department of Earth and Planetary Sciences, University of New Mexico, Albuquerque, New Mexico, USA
[12]Department of Chemistry, Fordham University, Bronx, New York, USA
[13]Department of Earth and Planetary Sciences, American Museum of Natural History, New York, New York, USA
[14]Space Sciences Laboratory, University of California, Berkeley, Berkeley, California, USA
[15]Department Physics and Astronomy, Purdue University, West Lafayette, Indiana, USA
[16]Department of Earth, Atmospheric and Planetary Sciences, Purdue University, West Lafayette, Indiana, USA
[17]Department of Physical Sciences, Kingsborough Community College, Brooklyn, New York, USA
[18]Department of Physics, Catholic University of America, Washington, D.C., USA
[19]Center for Research and Exploration in Space Science and Technology, NASA/GSFC, Greenbelt, Maryland, USA
[20]Department of Chemistry, University of Wisconsin-Madison, Madison, Wisconsin, USA
[21]Vatican Observatory, Vatican City State
[22]Curtin Institute for Radio Astronomy, Curtin University, Perth, Western Australia, Australia

***Correspondence**
Seamus L. Anderson, Space Science and Technology Centre, School of Earth and Planetary Sciences, Curtin University, GPO Box U1987, Perth, WA, Australia.
Email: seamus.l.anderson@gmail.com

(Received 16 July 2024; revision accepted 01 September 2026)

Abstract–The Dingle Dell meteorite fell in the wheat belt of Western Australia on Halloween night (October 31st) in 2016 and was observed by multiple cameras from the Desert Fireball Network, being recovered less than a week later. In this paper, we report the in-depth characterization and reclassification of this meteorite, from its original LL6 class to an updated L6 chondrite. Dingle Dell is an unbrecciated L6 chondrite with low shock features (S2) and no weathering (W0). The silicate mineral chemistry is typical of an L chondrite (Fa = 24.4 ± 0.3; Fs = 20.5 ± 0.2; Wo = 1.6 ± 0.3; all mol%), while the kamacite-Co concentration is on the high end of the L-chondrite range. The measured oxygen isotopes ($\delta^{17}O = 3.809 \pm 0.068$; $\delta^{18}O = 5.102 \pm 0.126$; $\Delta^{17}O = 1.115 \pm 0.011$) are slightly more consistent with an LL chondrite classification, though on the border shared by L and LL chondrites. The chromium isotopic anomaly measured in Dingle Dell also places it among both L and LL chondrites ($\varepsilon^{54}Cr = -0.37 \pm 0.09$). Analyses of cosmogenic radionuclides and noble gases indicate that Dingle Dell existed as a small meteoroid (10–15 cm radius) for 9.3 ± 1.3 Myr before impacting the Earth. Ideal gas pycnometry indicates a grain density of 3.61 ± 0.01 g cm^{-3} and a bulk density of 3.23 ± 0.02 g cm^{-3}, revealing a calculated porosity of 10.5% ± 0.5%. Dingle Dell's likely source region near the 3:1 mean motion resonance may constitute meteoritic sampling from an asteroid not associated with the Massalia or Flora families, the proposed sources for many L chondrites.

INTRODUCTION

The global collection of meteorites consists of over 70,000 samples, and while the overwhelming majority of these specimens do not have any information regarding their prior orbit, over 50 meteorites were photographically observed well enough when they fell to constrain their orbits prior to their collision with the Earth (Meier, 2024; https://www.meteoriteorbits.info/), making this small subset tremendously insightful for understanding the geochemical composition and structure of our solar system. Fireball camera networks (Devillepoix et al., 2020; Oberst et al., 1998; Spurný et al., 2006; Trigo-Rodríguez et al., 2006), which photograph and triangulate a passing fireball, are the best mechanism for expanding this catalog of meteorites with known orbital data. The Desert Fireball Network (DFN) is one such network, which currently extends across 30% of the landmass of Australia, over the states of Western and South Australia (Bland et al., 2012; Howie et al., 2017).

Dingle Dell (L6) is the fourth meteorite recovered by the DFN. Devillepoix et al. (2018) reported observations of a fireball over Morawa, Western Australia, just after 8 PM local time (UTC + 8) on the night of October 31, 2016, from which they were able to calculate a pre-collision orbit which had a semimajor axis of 2.254 ± 0.034 AU, an eccentricity of 0.5904 ± 0.063, and an inclination of 4.051° ± 0.012°. Their orbital modeling also shows that the meteoroid had a 6%, 12%, and 82% probability of originating from the 5:2, ν_6, and 3:1 resonances, respectively. The ν_6 secular resonance has previously been identified as a prominent delivery mechanism for LL chondrite material originating from the Flora (8) asteroid family (Vernazza et al., 2008), while the Gefion family may be producing L chondrites, delivering them via the 5:2 resonance (Nesvorný et al., 2009). Marsset et al. (2024) instead propose the Massalia asteroid family as the source of shocked L chondrites via the 3:1 resonance, due to spectral observations and collision modeling that suggest a family age of <500 Myr to match the ~470 Ma pressure–temperature event recorded in many L chondrites.

The Dingle Dell's meteoroid, which was estimated to have had an initial radius of 15 cm (Devillepoix et al., 2018), began ablating at an altitude of 81 km while traveling at 15.44 km s^{-1}, eventually ending its bright-flight phase at an altitude of 19 km, having slowed to 3.2 km s^{-1}. A four-person team recovered the meteorite 6 days later (November 6, 2016), from an open field near the Dingle Dell farm, approximately 130 m from the predicted fall line (Devillepoix et al., 2018). Local meteorological reports indicated that there had been no precipitation in the area between the fall and recovery of the meteorite.

The Dingle Dell meteorite (Figure 1) was first characterized by Benedix et al. (2017) and consists of a single, rounded brick-shaped rock measuring approximately 16 × 9 × 4 cm, with a mass of 1.15 kg. Apart from some accumulated dust that was initially on the surface of the meteorite, there is no evidence of terrestrial alteration from naked eye inspection or thin section imaging (see Results). Although Dingle Dell has an intact fusion crust covering the entire surface of the rock, one side has a sharp, blocky edge, which suggests a minor atmospheric breakup event, further supported by an eyewitness account and observations of the fireball. The cut surface (Figure 1) reveals a light interior with some indistinct chondrules.

This meteorite was originally classified as an LL6 chondrite in Meteoritical Bulletin 106 (Gattacceca et al., 2019). The previously measured olivine and pyroxene compositions showed intermediate values between those expected for an L or LL chondrite (Benedix et al., 2017), Dingle Dell's oxygen isotopes were more representative of an LL chondrite, hence its previous classification. Here, we present a more complete characterization of this specimen including updated electron microprobe measurements and optical

FIGURE 1. The Dingle Dell meteorite, displaying its cut surface and fusion crust. The red color on the fusion crust is dust contamination, not terrestrial alteration.

microscopic imaging which suggest that Dingle Dell is an L6 chondrite.

METHODS

We allocated samples of this meteorite to a consortium of scientists for a more complete coordinated analysis. Each of the analytical methods we used to characterize Dingle Dell as well as the sample used and at which institution they were performed are listed in Table 1.

Optical Microscopy

A polished thin section of Dingle Dell was examined for shock features using a Leica optical microscope with a rotating stage in both transmitted (planar and polarized) and reflected light. We imaged this using a Zeiss Axio Imager 503 (color), using its corresponding software to stitch the images into a mosaic.

X-Ray Computed Tomography (μCT)

CSIRO

The whole-rock sample of Dingle Dell was scanned using a Siemens SOMATOM medical scanner (220 × 220 × 100 μm voxel-edge^{-1}) at the Australian Resources Research Centre. The instrument was calibrated using air and a set of five standards of known density (2.7 to 4.3 g cm^{-3}) and the measurements were performed under an accelerating voltage of 140 kV and a beam current of 1 A. The data were processed using techniques developed for mineral applications (Godel, 2013; Godel et al., 2006).

AMNH

A 78 g wedge of Dingle Dell was cut and subjected to both fine-resolution CT as well as ideal gas pycnometry (see below). The wedge was scanned at the American Museum of Natural History using a GE Phoenix V|tome|x s240 μCT system, at a resolution of 19.5 μm voxel-edge^{-1}. This resolution enabled us to measure the magnitude of metal grain foliation or compression of a common axis across grains (Friedrich et al., 2008; Friedrich & Rivers, 2013), which produces a numerical anisotropy strength factor: C (Woodcock, 1977; Woodcock & Naylor, 1983) which can indicate the meteorite's shock state.

Ideal-Gas Pycnometry

We measured the bulk and grain volume of the same 78 g wedge that was analyzed via fine-resolution CT (AMNH). Bulk volume (and density) was measured by 3-D laser scanning using a NextEngine model 2020i Scanner HD. The scans were aligned, individually trimmed of artifacts, and fused to form a watertight mesh, the volume of which was calculated using Geomagic Verify Viewer. Grain volume (and density) was measured via ideal gas pycnometry using a Quantachrome Ultrapyc 1000 pycnometer which was running gaseous N_2 as the medium, but otherwise following the procedure described in Macke (2010).

Magnetic Susceptibility

Magnetic susceptibility was measured with a ZH-Instruments SM-30 meter, with volumetric

TABLE 1. Sample allocations and methods used in this study, listed by institution.

Science goal	Method and analysis	Institution	Sample
Shock state	Optical microscopy	Curtin University	Thin section
Shock state and density	X-ray computed tomography (μCT)	CSIRO—Kensington (Coarse resolution)/American Museum of Natural History (AMNH; Fine resolution)	Whole rock/78 g wedge
Density and porosity	Gas pycnometry & laser scanning (density and porosity)	Vatican observatory	78 g wedge (same sample used for CT)
Petrologic type and meteorite class	Scanning electron microscopy (SEM-EDS)	Curtin University/John de Lauter Centre	Thin section
	Electron microprobe (EPMA)	University of Western Australia	Thin section
Meteorite class	X-ray Powder Diffraction	Kingsborough Community College	197 mg chip
Oxygen isotope composition	Laser-assisted fluorination	University of New Mexico	186 mg chip
Cr isotope composition	Thermal ionization mass spectrometry (TIMS)	University of California—Davis	186 mg chip (same as oxygen isotope)
Bulk chemistry	Inductively coupled mass spectrometry (ICP-MS)	Fordham University	885 mg chip
Amino acid and organic composition	Amino acid analysis	NASA Goddard Space Flight Center	293 mg meteorite chips & 433 mg soil sample
Cosmic ray exposure (CRE) and meteoroid size	Noble gas analysis	ETH Zurich	37.1 and 27.1 mg chips
Cosmic ray exposure (CRE) and meteoroid size	Cosmogenic radionuclides	University of California—Berkeley/Purdue University	1.28 g chip

corrections according to the relation described in Gattacceca et al. (2004) and further corrections for sample geometry based on the schema of Macke (2010).

Scanning Electron Microscope Energy-Dispersive X-Ray Spectroscopy (SEM-EDS)

We determined Dingle Dell's modal mineralogy by imaging a thin section using a Tescan Integrated Mineral Analyzer housed in the Digital Mineralogy Hub of the John de Laeter Centre at Curtin University. This instrument was not programmed to automatically detect mineral phases in meteorites from the energy-dispersive X-ray spectra, so we constructed mineral phase maps from elemental abundance maps. We then determined modal mineral abundance using the techniques described by Ford et al. (2008) and Anderson (2023).

Electron Microprobe Analysis (EPMA)

Using the same thin section analyzed via SEM-EDS and optical microscope, we determined the mineral compositions of olivine, orthopyroxene, chromite, kamacite, and taenite. This was completed with a JEOL 8530F electron microprobe at the Centre of Microscopy, Characterization, and Analysis at the University of Western Australia. The probe was operated with an accelerating voltage of 20 kV and beam current of 20 nA, using the following standards: periclase (Mg), sodium niobate (Na), orthoclase (K (and Si for chromite only)), synthetic corundum (Al), Ti metal, Cr metal (olivine and pyroxene only), Tiebaghi chromite (chromite only), Mn metal, NMNH magnetite (Fe, chromite only), Fe metal (olivine, pyroxene, metals), Willsboro wollastonite (Ca), Ni metal, and Co metal.

X-Ray Powder Diffraction (XRD)

A 197 mg chip of Dingle Dell was powdered to <35 μm for XRD analyses and 150 mg was packed into a circular aluminum well with the sharp edge of a spatula in an attempt to ensure random grain orientations. XRD data were collected on an ARLTM Equinox 3000 position-sensitive detector X-ray diffractometer, irradiated with a beam of CuKα radiation, and restricted to a size of 0.24 × 5.00 mm using a slit system and the incidence angle of 6°. Meteorite data were collected for 120 min, and mineral standards were collected for 10 min each.

Phase quantification described in Howard et al. (2009) proceeds by initial identification of the phases present in the mixture pattern using the ICDD reference database. The identified phase-pure samples of the mineral phases are then selected from the lab's databank, analyzed under identical conditions as the meteorite, and their diffraction patterns are used in pattern fitting to arrive at modal abundances. To do this, the time normalized standard diffraction pattern (100% single phase) is reduced in intensity by a proportion/pattern fit factor to resolve a best-fit match to its intensity in the mixture pattern and is subtracted to leave a residual pattern. This process is repeated for all phases identified; a residual of zero counts indicates that all phases in the mixture are accounted for. The determined pattern fit proportions are not the actual phase proportions in the mixture until the component phases in the mixture are corrected for their relative differences in X-ray absorption. X-ray absorption values are calculated from phase compositions the values given in international tables for X-ray crystallography.

Laser-Assisted Fluorination (Oxygen Isotopes)

Oxygen isotope analyses were performed by CO_2 laser-fluorination dual inlet mass spectrometry at the University of New Mexico Institute of Meteoritics (Sharp, 1990). First, samples were crushed and then acid-treated (6 N HCl at 70 °C for 3 min, 3 times, followed by 3 rinses with 18 MOhm water, then dried at 70 °C) in order to remove possible terrestrial weathering products.

Samples (0.6–2.0 mg) were placed into Ni sample plates, which were placed in the vacuum chamber of the extraction line, pumped under high vacuum, and heated by an IR-lamp for a minimum of 16 h at room temperature in order to completely outgas the samples and remove potential moisture. Samples were then pre-fluorinated (BrF_5) in order to clean the stainless steel system and to react residual traces of water or air in the fluorination chamber. Molecular oxygen was released from the samples by laser-assisted fluorination (50 W infrared CO_2 laser) in an ~100 mbar BrF_5-atmosphere, producing molecular O_2 gas, SiF_4 gas, and solid fluorides. Excess reagent and gaseous SiF_4 were separated from O_2 by cryogenic trapping at −196 °C and reaction with hot NaCl. The molecular oxygen was purified by adsorbing onto a 13 Å molecular sieve at −196 °C, followed by elution of the O_2 from the first sieve at ~300 °C into a He-stream that carries the oxygen through a gas chromatography (GC) column (separation of O_2 and NF_3, a possible interference with the ^{17}O measurement) to a second 13 Å molecular sieve at −196 °C. After removal of the He, the O_2 was then released directly into a dual inlet isotope ratio mass spectrometer (Thermo Finnigan MAT 253 Plus).

The oxygen isotope ratios were calibrated against the isotopic composition of San Carlos olivine. Each sample analysis consists of 20 cycles of sample-standard comparison, and olivine standards were analyzed daily. Oxygen isotopic ratios were calculated using the following procedure: The $\delta^{18}O$ values refer to the per-mil deviation in a sample ($^{18}O/^{16}O$) from standard mean ocean water (SMOW), expressed as $\delta^{18}O = [(^{18}O/^{16}O)_{sample}/(^{18}O/^{16}O)_{SMOW}\text{-}1] \times 1000$. The delta values are converted to linearized values by calculating: $\delta^{18}O/^{17}O' = \ln[(\delta^{18}O/^{17}O + 1000)/1000] \times 1000$ in order to create straight-line mass-fractionation curves. The $\Delta^{17}O'$ values were obtained from the linear δ values by the following relationship: $\Delta^{17}O' = \delta^{17}O' - 0.528 \times \delta^{18}O'$, $\Delta^{17}O'$ values of zero define the terrestrial mass-fractionation line. $\Delta^{17}O'$ values lying on any line with a slope of ~0.52–0.53 are due to mass-dependent processes. Typical analytical precision of the laser-fluorination technique is better than ±0.01‰ for $\Delta^{17}O$. The aliquots for both oxygen and chromium (see below) isotopic analyses were sourced from separate regions of the meteorite, each of which were also separate from the CT subsample.

Thermal Ionization Mass Spectrometry (TIMS)

For Cr isotopic analyses, a small interior chip of Dingle Dell was crushed using an agate mortar and pestle. A total powdered mass of 18.17 mg was transferred into a Parr digestion vessel PTFE capsule along with a 3:1 mixture of ultrapure $HF{:}HNO_3$. The insert was sealed in a stainless steel jacket and heated in an oven for 96 h at 190 °C. After dissolution was complete, the sample solution was dried and then treated with alternating redissolution in 6 N HCl and concentrated HNO_3 to breakdown any fluorides formed during the high pressure–temperature dissolution step. Chromium was separated from the sample matrix using a 3-column separation procedure described in Yamakawa et al. (2009).

The isotopic composition of the purified Cr fraction was measured using a Thermo Triton Plus thermal ionization mass spectrometer. The Cr was loaded in 3 mg aliquots onto four outgassed W filaments for a total Cr amount of 12 mg. The four filaments containing Cr were bracketed with W filaments, two on each side, loaded with the standard: NIST SRM 979 (also with 3 mg Cr loads). Details on the mass spectrometry procedure are described in Sanborn et al. (2019). The Cr isotopic data are reported as parts per 10,000 deviation (ε-notation) from the NIST SRM 979 analyzed in the same analytical session.

Inductively Coupled Plasma Mass Spectrometry (ICPMS)

We performed elemental analysis on five chips of Dingle Dell (131.7, 116.5, 126.4, 123.4, 128.4 mg). We first ground each chip in an agate mortar and pestle. To dissolve the powders, we used a combination of HF and HNO_3 in a high-pressure CEM Mars 5 microwave digestion system, dried the resulting mixture to incipient dryness on a hotplate, treated the residue with $HClO_4$, and again dried it to incipient dryness to dissolve the samples. In addition to the Dingle Dell samples, a procedural blank and the Allende Standard Reference Meteorite (Jarosewich et al., 1987). The dissolved samples were taken up in 1% HNO_3 and analyzed with a ThermoElemental X-Series II ICPMS with the methods outlined in Friedrich et al. (2003) for trace elements and Wolf et al. (2012) for major and minor elements.

Amino Acid Analysis

Amino acids were analyzed at NASA Goddard Space Flight Center. Sample-handling tools, ceramics, and glassware were all rinsed with Millipore Integral 10 UV (18.2 MΩ cm, <3 parts-per-billion (ppb) total organic carbon) ultrapure water, wrapped in aluminum foil, and heated in air at 500 °C for at least 18 h to clean them of organic material. Most of the chemicals used were purchased from Fisher Scientific, Sigma-Aldrich, or Acros Organics. To prepare standard solutions for chromatographic analysis, individual compounds were dissolved in water and then combined to enable their measurement in a single chromatographic separation. Solutions of sodium borate were prepared from solid sodium tetraborate decahydrate (Sigma Ultra, 99.5%–100% purity) that was heated in air at 500 °C for 3 h prior to dissolution in water. All other solutions were prepared as described by Glavin et al. (2006). Samples were crushed into a powder using a clean mortar and pestle in an ISO 5 Labconco laminar flow hood under HEPA-filtered positive pressure. Procedural reagent blanks were processed in parallel to the meteorite samples as controls. Samples of Dingle Dell, along with separate soil samples collected at the fall site, were weighed and dissolved in 1 mL of ultrapure water then extracted in flame-sealed ampoules at 100 °C for 24 h. The samples were then split into two equal portions for a hydrolyzed portion and an unhydrolyzed portion. The samples were then dried via centrifugal evaporation. The hydrolyzed portion was hydrolyzed over 6 M HCl vapor for 3 h at 150 °C. The acid-hydrolyzed water extracts were desalted using cation-exchange resin (AG50W-X8, 100–200 mesh, hydrogen form, BIO-RAD), and the amino acids recovered by elution with 2 M NH_4OH (prepared from ultrapure water and NH AirProducts, in vacuo). The remaining half of each water extract (non-hydrolyzed fraction) was taken through the identical desalting procedure in parallel with the acid-hydrolyzed extracts to determine the free amino acid abundances in the meteorites. Free amino acids refer to those organic water-soluble species that are obtained without acid treatment; the total extract consists of both the hydrolyzable and free material. The final hydrolyzed and non-hydrolyzed samples were dried and then brought back up in 100 μL of ultrapure water. Of that sample, 10 μL was used for analysis.

The amino acids in the NH_4OH eluates were derivatized with o-phthaldialdehyde/N-acetyl-L-cysteine (OPA/NAC) for 15 min at room temperature. The abundance, distribution, and enantiomeric compositions of the two- to six-carbon aliphatic primary amine amino acids present in the non-hydrolyzed and acid-hydrolyzed water extracts were then determined by ultra-high performance liquid chromatography fluorescence detection and time of flight mass spectrometry (hereafter LC-FD/ToF-MS) using a Waters ACQUITY H Class UPLC with fluorescence detector and Waters Xevo G2 XS. The instrument parameters and analytical conditions used were similar to those described elsewhere (Glavin et al., 2006, 2010). For the Xevo mass calibrations, an automatically applied lockmass of a fragment of Leucine Enkephalin (278.1141 Da) with a scan time of 1 s every 60 s of elution time was used. The capillary voltage was set to 1.2 kV. The amino acids and their enantiomeric ratios were quantified from the peak areas generated from both fluorescence detection and from the mass chromatogram of their OPA/NAC derivatives as described previously in Glavin et al. (2006).

Noble Gas Analysis

Noble gas concentrations were measured at ETH Zürich, where we measured two chips (DD-NG-L, 37.1 mg; DD-NG-S, 27.1 mg) of Dingle Dell, wrapped in Al foil and loaded into the sample holding chamber of a crucible attached to an in-house built (sector field, Baur-source) noble gas mass spectrometer (Riebe et al., 2017). After heating the samples for 2 days to 110 °C, the sample gas was extracted by total melting in the Mo-crucible heated by electron bombardment and analyzed based on a protocol described in detail in Meier et al. (2017). Blank contributions were <0.1% for ^{3,4}He, <8% for ^{20,21,22}Ne, and <1.5% for ^{40}Ar. For DD-NG-S, a very high blank contribution (~75%) on ^{36}Ar left us no choice but to discard the Ar data. For DD-NG-L, the blank contribution is lower (25% on ^{36}Ar, 11% on ^{38}Ar), allowing us to derive both a cosmogenic ^{38}Ar concentration and an upper limit for the atmospheric (i.e., non-radiogenic) contribution to ^{40}Ar using the measured $^{40}Ar/^{36}Ar$ ratio. For the determination of the $^{22}Ne/^{21}Ne$-^{22}Ne, $^{22}Ne/^{21}Ne$-^{3}He cosmic-ray exposure ages, and cosmogenic $^{4}He/^{3}He$ ratios (used to calculate the radiogenic ^{4}He concentrations), we use the empirically calibrated, shielding-correcting production rate functions from Dalcher et al. (2013).

Cosmogenic Radionuclides

We gently crushed a fragment of ~1.29 g and removed ~100 mg of small pieces with attached fusion crust. The remaining sample was further crushed to a grain size of <0.5 mm and separated into a magnetic (metal) fraction of ~95 mg and a non-magnetic (stone) fraction of ~1.06 g. The metal fraction was purified in a two-step procedure using ultrasonic agitation in (1) 0.2 N HCl to remove attached troilite and (2) concentrated HF to dissolve attached silicates. The second step also dissolves some of the metal itself. The 80 mg of metal that remains after the first step corresponds to a bulk metal content of 6.7 wt%, which is closer to L chondrites than LL chondrites (Jarosewich, 1990). The 74.4 mg of purified metal that remained after the second step was used for radionuclide analysis.

We dissolved 91 mg of the stone fraction—along with a solution containing 2.94 mg of Be carrier and 3.69 mg of Cl carrier—in concentrated HF/HNO_3 in a Parr teflon digestion bomb placed inside an oven at 125 °C for 24 h. After the solution cooled, we separated the Cl fraction as AgCl, removed Si as SiF_4, and dissolved the residue in dilute HCl. A small aliquot was taken for chemical analysis by ICP-OES, and an additional 5.0 mg of Al carrier was added to the remaining solution to dilute the $^{26}Al/Al$ ratio to <3 × 10^{-11}. The metal fraction was dissolved in dilute HNO_3 along with a carrier solution containing 1.48 mg of Be, 1.66 mg of Al, and 4.90 mg of Cl. After dissolution, we took a small aliquot (~3.3%) of the dissolved sample for chemical analysis (Mg, Fe, Co, Ni) by ICP-OES. The measured concentration of ~140 ppm Mg in the dissolved metal sample indicates that the amount of silicate contamination in the purified metal is relatively small (~0.08 wt%).

After taking a small aliquot of the dissolved metal and stone samples for chemical analysis, we used the remaining solutions for radionuclide separation following procedures described in Welten et al. (2011). After separating and purifying the Be, Al, and Cl fractions, the $^{10}Be/Be$, $^{26}Al/Al$, and $^{36}Cl/Cl$ ratios of these samples were measured by accelerator mass spectrometry (AMS) at Purdue University's PRIME Lab (Sharma et al., 2000). The measured ratios were normalized to those of well-characterized AMS standards (Nishiizumi, 2004; Nishiizumi et al., 1990, 2007; Sharma et al., 1990) and converted to concentrations in disintegrations per minute per kg (dpm/kg). The ^{10}Be and ^{26}Al concentrations in the metal fraction were corrected for small contributions of ^{10}Be (0.2%) and ^{26}Al (1.0%) from the stone fraction.

RESULTS

Optical Microscopy

The texture present in Dingle Dell's thin section is characterized by chondrules with poorly defined boundaries set in a recrystallized matrix (Figure 2). Mineralogy consists of olivine, orthopyroxene, metal, and sulfide, with minor amounts of plagioclase, clinopyroxene, phosphate, and chromite. Most of the plagioclase grains exceed 150 μm in size. These features are typical of an equilibrated ordinary chondrite. Shock features are mild (S2) (Stöffler et al., 2018), as olivine and orthopyroxene exhibit very slight undulose extinction, but the olivine portions have no planar fractures. Dingle Dell exhibits no features of terrestrial weathering in the thin section (W0), as metal grains are pristine with no oxidized rims.

Ideal Gas Pycnometry & Laser Scanning

Macke et al. (2017) reported a bulk density of 3.23 ± 0.02 g cm^{-3} and a grain density of 3.61 ± 0.01 g cm^{-3}, measured from the 78 gm wedge of Dingle Dell. Grain density (which is dependent solely on mineralogy) is closer to the average of the range of L chondrite falls (3.58 g cm^{-3}) reported by Macke (2010) than it is for the average of LL falls (3.52 g cm^{-3}), with a similar tale for bulk density (Figure 3). However, the bulk and grain densities of Dingle Dell do fall within the ranges of both populations (Consolmagno et al., 2008). Porosity P, calculated from bulk and grain densities (ρ) by the equation $p = 1 - (\rho_{bulk}/\rho_{grain})$, yields a porosity of (10.5 ± 0.5)%. This is slightly higher than average for L falls (as expected for freshly collected specimens) but consistent with both L and LL fall populations, according to data in Macke (2010).

Magnetic Susceptibility

Macke et al. (2017) also report a magnetic susceptibility of log χ = 4.78 ± 0.09, which is low though still within the expected range for L chondrites (4.87 ± 0.10; Rochette et al., 2003; Consolmagno et al., 2006; see Figure 3).

FIGURE 2. Transmitted light image of Dingle Dell's thin section. Although a crack can be seen on the left side of the sample, this thin section does not exhibit signs of brecciation or significant shock. Although occasional distinct chondrules can be seen (such as in the center and upper right corner), most are poorly defined and often difficult to distinguish from the matrix.

CT

The coarse resolution CT (220 × 220 × 100 µm voxel^{-1}) of the whole rock reveals a distribution of high-density metal and sulfide consistent with an ordinary chondrite. In the fine-resolution CT (19.5 µm per voxel-edge), mm-sized circular areas of lower, silicate density can also be seen which we identify as chondrules (Figure 4). At this finer resolution, Dingle Dell does not appear to be brecciated or have distinctive clasts; however, this level of detail is still insufficient to identify or dismiss any possible micro-cracks. A grain density of 3.45 g cm^{-3} was calculated from the coarse CT data.

A typical slice of the tomographic volume from the fine-resolution µCT (19.5 × 19.5 × 19.5 µm voxel^{-1}) of the 78 g wedge is shown in Figure 3. Little intergranular porosity can be distinguished at this resolution; therefore, the 10.5% porosity in Dingle Dell, determined by Ideal gas Pycnometry, is probably in the form of microcracks, which requires a resolution of ~2–3 µm voxel-edge^{-1} to detect. From the µCT data, we were able to calculate the collective shape orientation of the metal grains in Dingle Dell, which indicates a mild degree of compaction which is plausible for its porosity (Figure 5), compared to other meteorites (Friedrich et al., 2017).

SEM-EDS

The mineral map from the SEM-EDS measurements indicates that the mineralogy of Dingle Dell is dominated by relict chondrules, Fe-Ni metal, Ca-phosphates, chromite, and sulfides embedded in a recrystallized silicate matrix. Major minerals include olivine, pyroxene, plagioclase, troilite, kamacite, and taenite. Chromite and phosphates are also present, though in minor amounts. A false-color mineral phase map of Dingle Dell, taken from one of the polished thin sections, is shown in Figure 6. The modal mineral abundances were measured using the python machine learning approach described in Anderson (2023), and are listed in Table 2, and plotted in Figure 7 (black stripes) along with the XRD measurements (see below). Using Fiji/ImageJ, we measured an average chondrule diameter of 0.9 ± 0.3 mm (n = 12), though due to its higher petrologic type, smaller chondrules were more difficult to distinguish; therefore, our measured average is likely higher than the true average.

XRD

The PSD-XRD pattern for Dingle Dell is dominated by sharp high-intensity diffraction from olivine (Fo90),

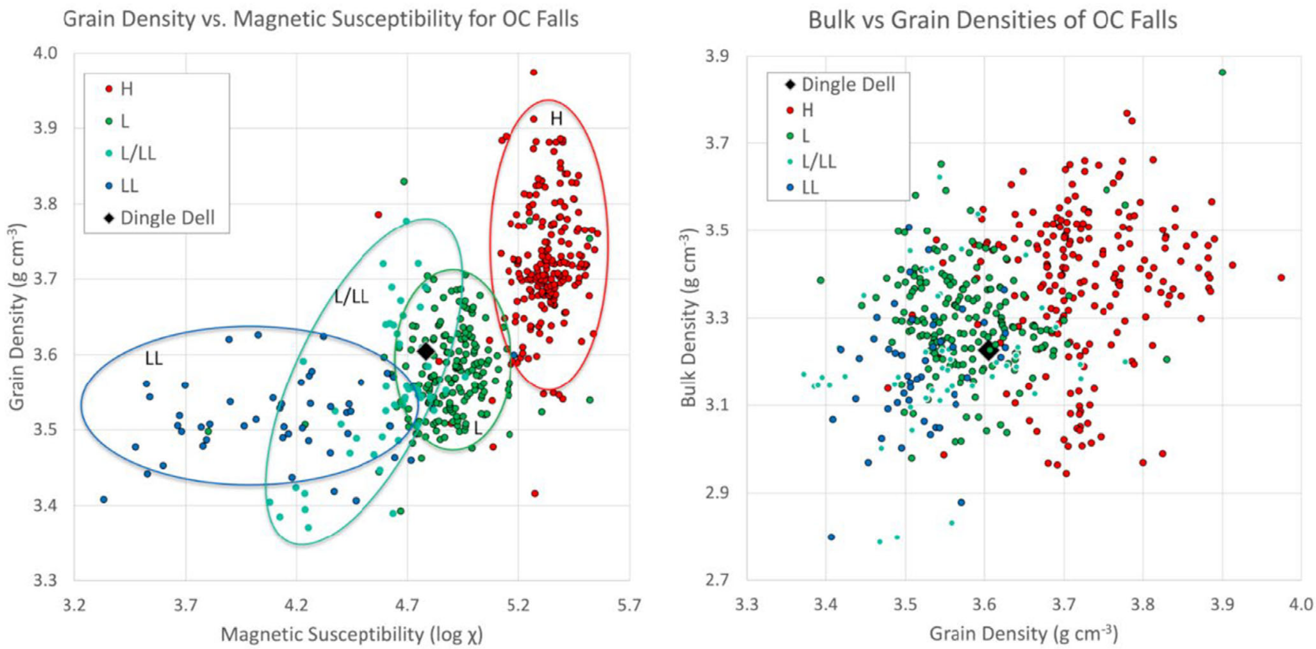

FIGURE 3. Dingle Dell's grain density and magnetic susceptibility plotted together (left) along with other ordinary chondrites (data from Macke (2010) and Macke (personal communications)). These broad groupings show that Dingle Dell could belong to either the L's or L/LL's based on magnetic susceptibility and grain density. The same population's bulk and grain densities are plotted on the right.

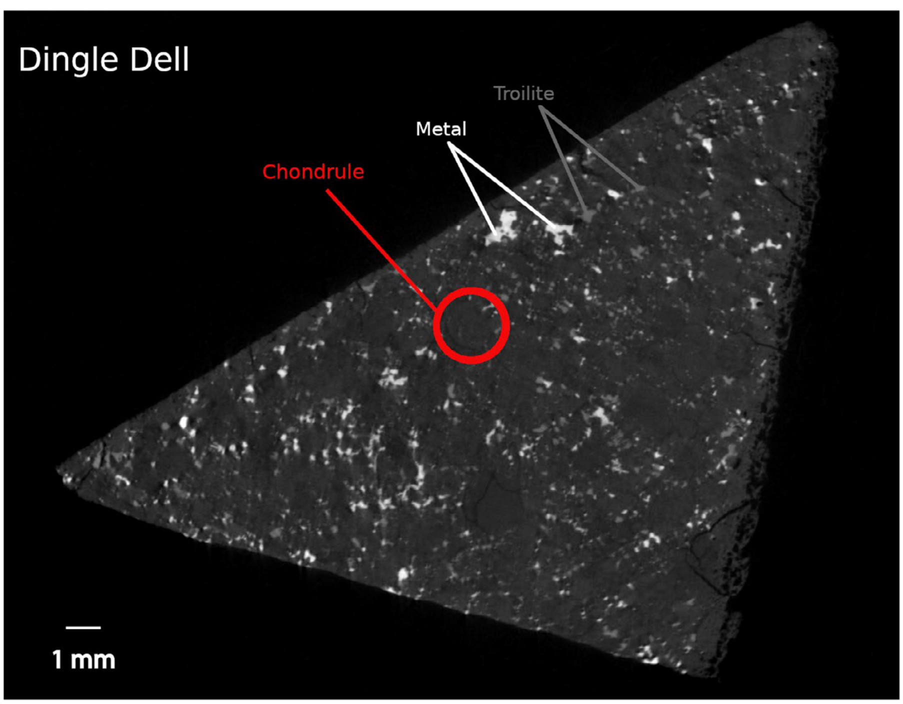

FIGURE 4. An X-ray μCT tomography or "slice" of a portion of Dingle Dell, collected at a resolution of 19.5 μm per voxel-edge. Areas with higher density (Fe-Ni metal) appear as white. Light gray portions have an intermediate density and are most likely chromite and troilite grains. Darker gray areas, which comprise most of the sample, are silicates, where occasional circular features (chondrules) can be seen. The surrounding black is air. Note the right edge of this sample is fusion crust.

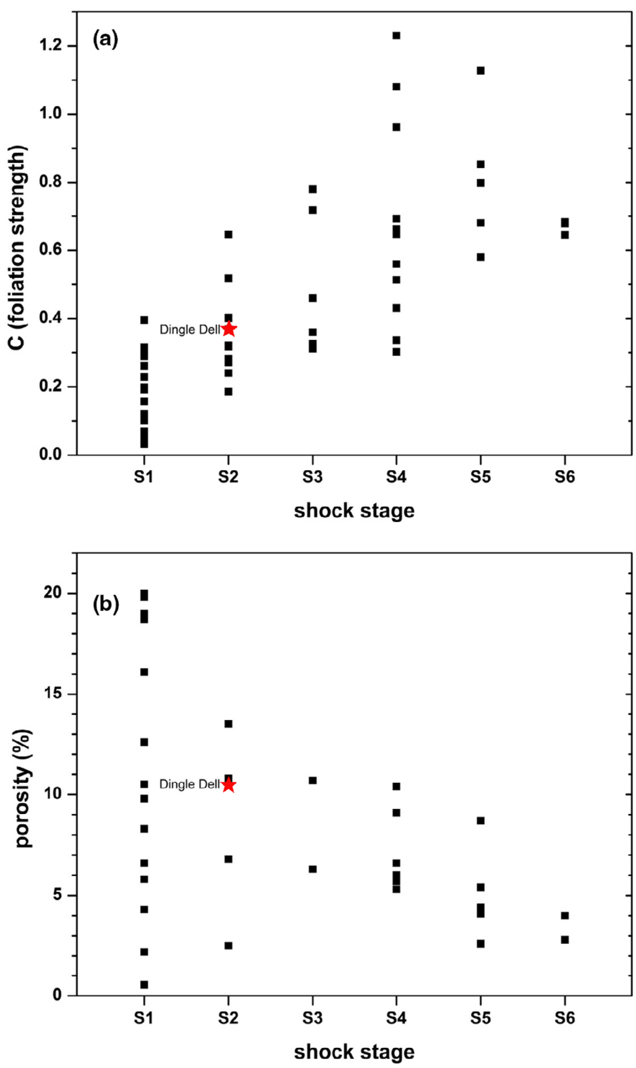

FIGURE 5. (a) Degree of preferred shape orientation (foliation) of metal grains versus petrographic shock stage. (b) Porosity versus petrographic shock stage. Other ordinary chondrite data points are from previous work by Friedrich et al. (2017).

pyroxene (enstatite), and feldspar along with minor diffraction peaks from Fe-Ni metal and sulfide. The pattern shows little evidence for noise resulting from fluorescence induced by interaction of Cu-radiation with Fe-oxides, consistent with Dingle Dell being a rapidly recovered fall. The modal mineralogy data determined by both XRD and SEM-EDS measurements are listed in Table 2.

The mineral abundances for Dingle Dell, obtained via XRD and SEM-EDS, are plotted next to the average abundances for both the L and LL chondrite groups in Figure 7. Data for the L and LL group averages are taken from Dunn et al. (2010).

EPMA

The mineral chemistries of chromite, olivine, orthopyroxene, and Fe-Ni metal measured in Dingle Dell's thin section are listed in Table 3. The average olivine and orthopyroxene compositions are plotted against other orbital L, LL, and L/LL meteorites in Figure 8 and are as follows (in mol%): Fa = 24.4 ± 0.3 (n = 21); Fs = 20.5 ± 0.2 (n = 22); Wo = 1.6 ± 0.3 (n = 22). The average chromite compositions are as follows: Cr/(Cr + Al) = 0.869 ± 0.004 (n = 11); Fe/(Fe + Mg) = 0.872 ± 0.007 (n = 11). The average Ni and Co concentrations in kamacite are 6.43 ± 0.30 wt% and 0.99 ± 0.22 wt%, respectively (n = 14), while those in taenite are 24.9 ± 1.8 (Ni) and 0.508 ± 0.10 wt% (Co; n = 6). The average TiO_2 concentration in Dingle Dell's measured chromite grains is 2.84 ± 0.23 wt%. These mineral compositions indicate that Dingle Dell is an L chondrite (Bunch et al., 1967; Scott et al., 1986; Kallemeyn et al., 1989; Rubin, 1990; see Figure 8). Combined with the petrologic texture, an L6 classification is more appropriate.

Bulk Chemistry

We present data from ICPMS on 49 major, minor, and trace elements plotted in Figure 9 and listed in Table 4. Errors based on the five analyzed replicates are typically <18% relative standard deviation, reflecting the heterogeneity of the different aliquots analyzed. Errors higher than that value are associated with elements that are associated with phosphate minerals (e.g., Th, U) or concentrated in metallic phases (e.g., Co, Ru) that are more difficult to sample representatively in the five ~100 mg sample chips we used. Lithophiles in Dingle Dell (Figure 9) have a mean and 1σ CI and Mg normalized abundance of 0.85 ± 0.06. Kallemeyn et al. (1989) demonstrated that ordinary chondrites possess a mean CI and Mg normalized lithophile abundance of 0.9, which suggests that Dingle Dell is an ordinary chondrite. Within the ordinary chondrites, total siderophile element content increases from LL → L → H. Siderophile elements in Dingle Dell (Figure 9) have a mean and 1σ CI and Mg normalized abundance of 0.71 ± 0.06, which is within errors of both the L and LL chondrite levels of identically normalized siderophile abundances.

The results of ICP-OES are listed in Table 5 and are more consistent with an L chondrite bulk chemistry than the ICP-MS measurements (see Figure 9, Table 4), specifically the concentrations of Ni (14 wt%) and Co (0.69%) in the purified metal fraction (Afiattalab & Wasson, 1980). Note that the bulk metal content (6.7 wt %) of the 1.3 g chip as well as the bulk metal

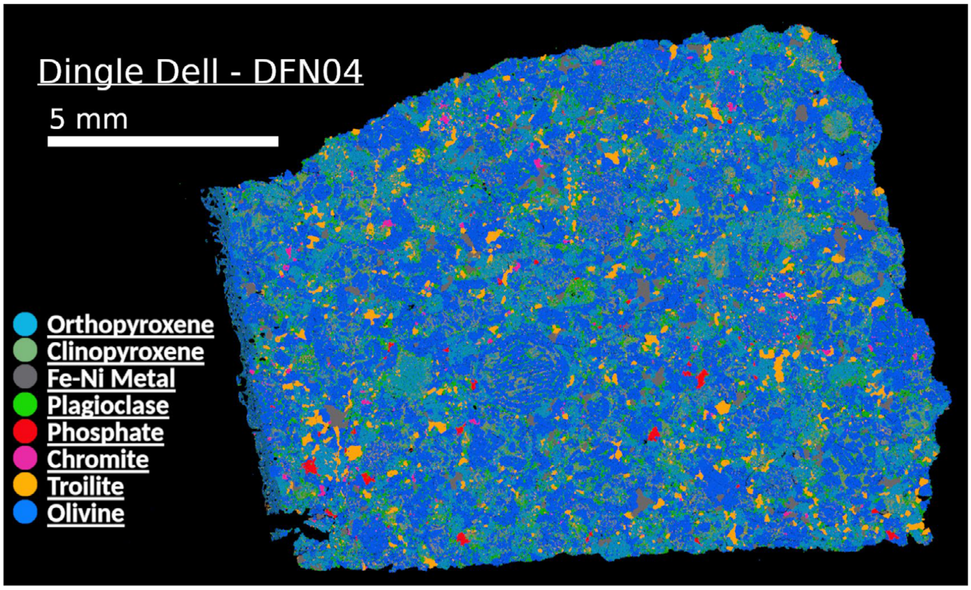

FIGURE 6. Mineral map of Dingle Dell's thin section constructed using SEM-EDS data. The texture seen here is typical of an equilibrated ordinary chondrite: metal and troilite grains along with poorly defined chondrules set within a recrystallized silicate matrix. Minor amounts of chromite and phosphate are also dispersed throughout the sample.

TABLE 2. Modal mineralogy of the Dingle Dell meteorite determined by XRD and SEM-EDS.

Method	Olivine	Orthopyroxene	Plagioclase	Sulfides	Metal
XRD vol%	54.5	27.7	12.9	3.3	1.6
XRD wt%	55.2	26.8	9.7	4.7	3.6
SEM wt%	47.3	28.5	11.4	5.4	5.8

Note: Weight percentages are based on assumed mineral densities (in g/cm^3) of 3.5 (olivine), 3.3 (orthopyroxene), 2.6 (plagioclase), 4.8 (troilite), and 7.8 (metal).

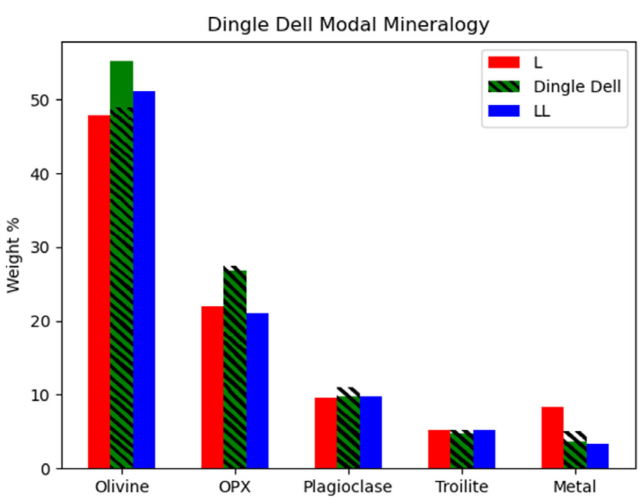

FIGURE 7. The modal mineralogy of the Dingle Dell meteorite (central bar, green for XRD, black stripes for SEM), as compared to the average values for both the L (left/red) and LL (right/blue) ordinary chondrite groups (Dunn et al., 2010).

composition (0.69 wt% Co and 14.0 wt% Ni) of the metal separated from this chip (both measured via ICP-OES) fall within the expected range for L chondrites (Afiattalab & Wasson, 1980; Jarosewich, 1990; Lodders, 2021), as does the bulk composition of this fragment (Table 5, Figure 9).

Oxygen Isotopes

Our three aliquots of Dingle Dell yielded oxygen isotope compositions of $\delta^{17}O = 3.809 \pm 0.068$; $\delta^{18}O = 5.102 \pm 0.126$; $\Delta^{17}O = 1.115 \pm 0.011$ (all 1σ). These values are plotted in Figure 1, along with oxygen isotopic values for other meteorites belonging to the H, L, and LL groups (data from Clayton et al., 1991). Compared to other ordinary chondrites, Dingle Dell's oxygen isotopes most closely align with LL chondrites, although they reside near the overlapping border between the L and LL groups.

TABLE 3. The EPMA measurements from Dingle Dell's thin section.

Point name	MgO	Na_2O	SiO_2	Al_2O_3	TiO_2	Cr_2O_3	FeO	MnO	CaO	K_2O	NiO	CoO	Total
Chromite													
Chromite 1	2.47	0.05	0.01	5.69	2.85	56.1	30.67	0.62	0	0	0	0.01	98.48
Chromite 2	2.35	0.07	0	5.61	2.82	56.22	30.71	0.65	0	0	0	0.01	98.43
Chromite 3	2.71	0	0	5.5	2.89	56.74	30.57	0.6	0	0.01	0	0.01	99.04
Chromite 4	2.57	0.02	0.01	5.76	2.78	56.54	30.22	0.66	0	0	0	0.02	98.58
Chromite 5	2.25	0.03	0.02	6.21	2.25	56.14	30.74	0.65	0	0.01	0	0.03	98.34
Chromite 6	2.44	0.02	0	5.74	2.92	56.45	30.68	0.62	0	0	0	0.03	98.91
Chromite 7	2.43	0.06	0.04	5.68	2.92	56.43	30.62	0.6	0	0	0	0.02	98.82
Chromite 8	2.61	0	0	5.52	3.1	56.46	30.36	0.62	0	0.01	0	0.03	98.71
Chromite 9	2.51	0.01	0	5.58	2.78	56.33	30.48	0.68	0	0	0	0.01	98.38
Chromite 10	2.52	0.04	0	5.55	3.1	56.54	30.83	0.58	0.06	0	0	0.02	99.25
Chromite 11	2.76	0.01	0.02	5.6	2.92	55.97	30.25	0.6	0	0	0	0.02	98.17
Olivine													
Olivine 1	38.2	0.01	38.48	0	0	0	22.74	0.42	0.01	0.01	0	0.04	99.9
Olivine 2	38.67	0.03	38.44	0	0.01	0	22.52	0.46	0.01	0	0	0.01	100.16
Olivine 3	38.7	0	38.3	0	0	0	22.18	0.47	0.01	0	0	0.03	99.69
Olivine 4	38.72	0.03	38.52	0	0	0	22.05	0.55	0	0	0	0	99.87
Olivine 5	38.86	0	38.48	0	0	0	22.17	0.51	0.01	0.01	0.01	0.02	100.08
Olivine 6	38.74	0	38.53	0	0	0	22.17	0.48	0.01	0	0.01	0.02	99.95
Olivine 7	38.32	0	38.3	0	0.01	0	22.65	0.42	0.01	0	0	0.02	99.74
Olivine 8	38.51	0.02	38.17	0	0.04	0.01	22.33	0.44	0	0	0	0.02	99.54
Olivine 9	38.54	0.01	38.23	0	0.02	0	22.19	0.43	0.01	0	0	0.01	99.42
Olivine 10	38.79	0	38.04	0	0	0.01	22.37	0.5	0.02	0.01	0.01	0.02	99.75
Olivine 11	38.08	0.03	38	0	0.04	0	22.89	0.51	0.05	0.01	0.01	0.01	99.62
Olivine 12	38.46	0.02	38.23	0	0.03	0	22.43	0.49	0.01	0	0	0.01	99.68
Olivine 13	38.45	0	38.36	0	0	0.01	22.61	0.51	0.02	0.01	0	0.03	100
Olivine 14	38.63	0.03	38.18	0	0.06	0.01	22.25	0.5	0.12	0.01	0	0.03	99.8
Olivine 15	38.58	0	38.54	0	0.06	0.02	22.42	0.42	0.01	0	0	0.01	100.08
Olivine 16	38.64	0.02	38.42	0	0	0	22.42	0.47	0	0	0	0.02	99.99
Olivine 17	38.43	0	38.41	0	0	0.01	22.74	0.41	0.02	0	0	0.01	100.04
Olivine 18	38.9	0	38.34	0	0	0	22.3	0.42	0.02	0	0	0.03	100
Olivine 19	38.61	0.01	38.32	0	0.01	0	22.23	0.45	0.01	0	0	0.02	99.66
Olivine 20	38.6	0	38.42	0	0.03	0	22.37	0.44	0.01	0	0.04	0.02	99.92
Olivine 21	38.52	0.01	38.11	0	0	0	22.45	0.45	0	0	0.01	0	99.56
Orthoyroxene (Opx)													
Opx 1	28.77	0.04	55.44	0.14	0.17	0.1	13.59	0.43	0.71	0	0	0	99.41
Opx 2	29	0.03	55.82	0.15	0.14	0.09	13.64	0.51	0.74	0	0	0	100.11
Opx 3	28.83	0.02	55.42	0.15	0.17	0.1	13.66	0.46	0.66	0	0.02	0	99.49
Opx 4	28.9	0	55.63	0.14	0.16	0.08	13.85	0.5	0.61	0.01	0.03	0.01	99.93
Opx 5	28.68	0.03	55.68	0.12	0.16	0.1	13.55	0.46	0.96	0	0	0.01	99.76
Opx 6	28.52	0.02	55.7	0.15	0.17	0.1	13.61	0.49	0.96	0.01	0	0	99.72
Opx 7	28.7	0.04	55.4	0.15	0.21	0.13	13.71	0.46	0.89	0.01	0	0	99.7
Opx 8	28.56	0.04	55.57	0.14	0.19	0.13	13.62	0.5	1.06	0	0	0	99.81
Opx 9	28.8	0.01	55.4	0.14	0.12	0.12	13.75	0.5	0.89	0	0.01	0.02	99.76
Opx 10	28.71	0.02	55.58	0.16	0.19	0.11	13.59	0.42	0.96	0.01	0.01	0	99.77
Opx 11	28.94	0.01	55.56	0.14	0.13	0.1	13.58	0.45	0.69	0	0	0	99.63
Opx 12	28.79	0.01	55.45	0.16	0.2	0.12	13.51	0.48	0.93	0	0.01	0.01	99.65
Opx 13	28.79	0.01	55.63	0.16	0.2	0.11	13.62	0.47	0.67	0	0	0	99.66
Opx 14	28.61	0.03	55.73	0.17	0.21	0.16	13.69	0.46	1.06	0	0	0.01	100.12
Opx 15	28.81	0.01	55.63	0.16	0.18	0.12	13.8	0.52	1.09	0	0	0.01	100.33
Opx 16	28.91	0	55.77	0.15	0.23	0.09	13.71	0.53	0.78	0	0.03	0.02	100.21
Opx 17	28.73	0.02	55.76	0.14	0.15	0.15	13.53	0.48	0.94	0	0	0.01	99.92
Opx 18	29.04	0	55.66	0.16	0.25	0.12	13.58	0.46	0.8	0	0	0.01	100.09
Opx 19	28.84	0.01	55.65	0.16	0.12	0.13	13.59	0.43	1.02	0	0	0.02	99.97

TABLE 3. *Continued.* The EPMA measurements from Dingle Dell's thin section.

Point name	MgO	Na_2O	SiO_2	Al_2O_3	TiO_2	Cr_2O_3	FeO	MnO	CaO	K_2O	NiO	CoO	Total
Opx 20	28.98	0	55.76	0.15	0.19	0.09	13.95	0.46	0.67	0	0.05	0.02	100.32
Opx 21	29	0.03	55.92	0.11	0.11	0.47	13.65	0.47	0.73	0	0.01	0.01	100.5
Opx 22	28.94	0	55.75	0.15	0.21	0.1	13.87	0.44	0.68	0	0.05	0	100.21
	Mg	Na	Si	Al	Ti	Cr	Fe	Mn	Ca	K	Ni	Co	
Kamacite													
Kamacite 1	0.01	0.01	0	0	0	0	93.8	0.03	0	0.01	6.15	1.1	101.11
Kamacite 2	0	0	0	0	0.01	0	95.01	0	0	0.01	5.77	1	101.82
Kamacite 3	0.01	0.01	0	0	0.02	0.01	93.28	0.01	0	0	6.54	1.02	100.89
Kamacite 4	0.01	0.01	0	0	0.04	0	92.99	0	0	0	6.45	0.87	100.38
Kamacite 5	0.01	0	0	0	0	0	94.62	0	0	0	6.38	0.53	101.53
Kamacite 6	0	0.01	0	0.01	0	0	93.24	0	0	0	6.02	1.56	100.85
Kamacite 7	0	0	0	0	0	0.01	93.07	0.01	0.01	0.01	6.93	0.93	100.97
Kamacite 8	0.01	0	0	0	0	0	93.13	0.01	0	0	6.55	0.93	100.63
Kamacite 9	0	0.01	0	0.01	0.01	0.01	93.7	0	0	0	6.26	0.93	100.93
Kamacite 10	0.01	0.02	0.01	0	0.03	0	92.91	0	0	0.02	6.55	1.2	100.75
Kamacite 11	0	0.02	0	0	0.01	0.01	93.25	0	0	0	6.41	0.99	100.7
Kamacite 12	0.01	0.03	0	0	0.02	0.01	94.08	0	0	0	6.68	0.89	101.71
Kamacite 13	0.01	0.05	0	0	0.02	0	92.98	0	0	0.01	6.64	1.02	100.73
Kamacite 14	0.01	0	0	0	0	0	92.91	0	0	0.01	6.64	0.91	100.48
Taenite													
Taenite 1	0.01	0.06	0.01	0.01	0	0.01	73.41	0.01	0	0	26.36	0.54	100.41
Taenite 2	0	0.01	0	0	0	0	73.73	0	0	0	26.07	0.35	100.17
Taenite 3	0.01	0.04	0.01	0	0	0.01	75.66	0	0	0	23.73	0.62	100.1
Taenite 4	0	0	0	0	0	0	77.94	0.01	0	0.01	21.87	0.52	100.36
Taenite 5	0.01	0	0	0	0	0	74.57	0	0	0	24.87	0.44	99.89
Taenite 6	0.01	0	0	0	0	0	73.56	0.01	0	0	26.24	0.57	100.4

Note: Chromite, olivine, and orthopyroxene compositions are reported in oxide wt%, while taenite and kamacite compositions are reported in elemental wt%.

TIMS (Chromium Isotopes)

The combined $\Delta^{17}O$ and $\varepsilon^{54}Cr$ data (Figure 10) indicate that Dingle Dell plots in the field of ordinary chondrites compared to the other literature data for LL, L, and H chondrites (Table 6, Figure 10). Although the oxygen isotopes suggest that Dingle Dell more closely aligns with an LL chondrite classification, chromium isotopes alone do not appear to be indicative of meteorite class, as shown with Novato's (L6) location in Figure 11 (Jenniskens et al., 2014).

Amino Acid Composition

Representative LC-FD chromatograms of the hot water extracts of the Dingle Dell meteorite, soil collected from the fall site, a procedural blank, and an amino acid standard mixture are shown in Figure 10. Amino acid identification was confirmed by comparison of the retention times of both UV fluorescence chromatogram and associated single ion mass chromatogram peaks in the meteorite, soil, and procedural blank data to the corresponding peaks observed in the amino acid standard. The peaks labeled "X" and "*" correspond to artifacts from the methodology that did not interfere with amino acid identification and quantification. The procedural blank-corrected abundances and D/L ratios (d- to l-enantiomer chiral abundance) of free amino acids in the Dingle Dell meteorite and soil water extracts are shown in Figure 11. The free amino acid abundances in the Dingle Dell meteorite were very low ranging from 0.002 to 0.7 nmol per gram and can mostly be attributed to terrestrial contamination from the landing site soil, which had a similar distribution of amino acids but present at a higher concentration. In addition, the D/L ratios of the protein amino acids detected in Dingle Dell were identical within error to the enantiomeric ratios of the same amino acids extracted from the landing site soil (Table 7), strongly suggesting a terrestrial origin for the amino acids in Dingle Dell. Nevertheless, it is possible that the Dingle Dell meteorite contains trace levels of amino acids of extraterrestrial origin, but they cannot be distinguished from the amino acids also present in the soil.

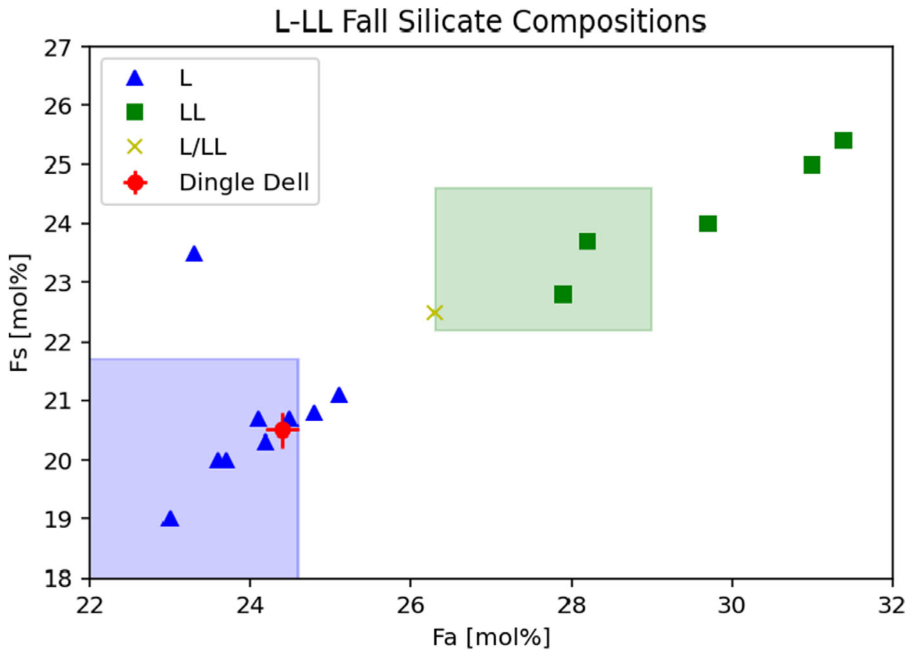

FIGURE 8. Olivine (fayalite; Fa) and pyroxene (ferrosilite; Fs) compositions for Dingle Dell and other L, LL, and L/LL chondrite falls with characterized orbits. The blue box represents the limits for L compositions and the green box represents the limits for LL compositions (Keil & Fredriksson, 1964). Data for individual meteorite compositions originates from: Bischoff et al. (2017); Popova et al. (2013); Spurný et al. (2014, 2016); Llorca et al. (2005); Jenniskens et al. (2014, 2019, 2020); Bouvier et al. (2017); Pratesi et al. (2021); Ferus et al. (2020); Kalasová et al. (2020); Brown et al. (2023); Smith (1980).

The total amino acid abundances are on the same order of magnitude as the free amino acids (Table 8). The only other ordinary chondrites where both hydrolyzed and unhydrolyzed amino acids have been reported are the LL3 Chainpur and Bishunpur meteorites (Chan et al., 2012). They showed comparable abundances of the amino acids in the unhydrolyzed fraction for the amino acids above detection limit (glycine, alanine, and glutamic acid) as Dingle Dell, but at least an order of magnitude more hydrolyzed than unhydrolyzed portion for these amino acids as well as several others not detected in the unhydrolyzed water extract. Considering that the potentially contaminated Dingle Dell hydrolyzed sample is less than an order of magnitude different from the unhydrolyzed sample gives confidence that the unhydrolyzed data are representative and perhaps any potentially present indigenous amino acids in Dingle Dell are most abundant in the free form, as is the case with many thermally altered carbonaceous chondrites (e.g., Burton et al., 2012, 2015). Carbon, hydrogen, and/or nitrogen isotope measurements of individual free amino acids in the Dingle Dell meteorite extracts would be required to more firmly establish a potential extraterrestrial origin.

Cosmogenic Radionuclides and Noble Gases

The concentrations of cosmogenic ^{10}Be, ^{26}Al, and ^{36}Cl (Table 9) in the stone fraction of Dingle Dell are on the low end of calculated production rates in objects with radii of 10–65 cm (Leya & Masarik, 2009). The ^{26}Al/^{10}Be ratios of ~2.8 in the bulk sample and 0.72 in the metal fraction imply that the radionuclides are saturated, indicating a CRE age >7 Ma, as is also shown by the noble gases (see below). Based on the calculated cosmogenic radionuclide production rates as a function of size and depth, we conclude that these low concentrations in the stone fraction of Dingle Dell are best explained by irradiation near the center of an object with a radius of 10–15 cm, although near surface irradiation in a larger object cannot be excluded. The relatively high ^{10}Be and ^{26}Al concentrations of 5.8 and 4.2 dpm/kg in the metal phase of Dingle Dell favor irradiation in a small object, with a radius of 10–15 cm. This pre-atmospheric size is roughly consistent with the photometrically predicted radius of 14–18 cm (38–82 kg) reported in Devillepoix et al. (2018). From the cosmogenic radionuclide data, we conclude that Dingle Dell had a simple, one-stage CRE history >7 Myr as a small object in space.

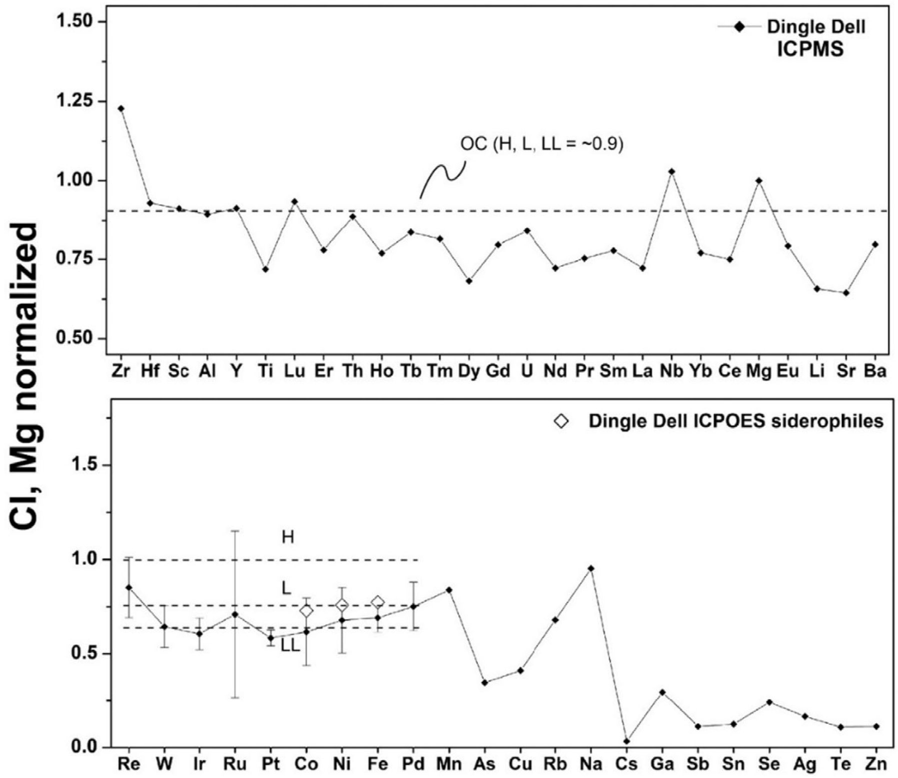

FIGURE 9. CI and Mg normalized elemental abundances for the Dingle Dell meteorite. The lithophile element content (top) clearly indicates that this meteorite is an ordinary chondrite with mean abundances close to the ordinary chondrite refractory lithophile mean of ~0.9. ICPMS-based siderophile elements (Re-Pd, bottom left) with inter-replicate errors from Table 4 are also shown with ICPOES determined siderophile abundances. Average Fe abundances for ordinary chondrite groups are shown as dotted lines (data from Lodders, 2021). The inventory of Dingle Dell's siderophile elements is akin to the L and LL chondrites. The siderophile abundances of the larger ICPOES (for cosmogenic radionuclide work) chip best match an L chondrite composition. CI data are from Lodders (2021).

The noble gas (He, Ne, and Ar) inventory of Dingle Dell is almost completely cosmogenic and radiogenic (Table 10). There are no solar wind gases, and only a marginal contribution of other trapped gases, mainly for Ar, and likely of Q origin (Busemann et al., 2000). The cosmogenic $^{22}Ne/^{21}Ne$ ratio of 1.160 ± 0.004 and the cosmogenic $^{3}He/^{21}Ne$ ratio of 6.29 ± 0.33 are compatible with exposure to galactic cosmic rays in a small meteoroid (radius approximately 10 cm), or alternatively, within the top 2 cm of the surface of a larger meteoroid, according to the models by Leya and Masarik (2009).

Using the production rates for ^{3}He, ^{21}Ne, and ^{38}Ar, calculated with the shielding-correcting production functions from Dalcher et al. (2013), we determine consistent cosmic ray exposure ages of 8.6 ± 0.5 and 8.7 ± 0.3 Myr for ^{3}He and ^{21}Ne (simple average of the two samples), respectively. While the ^{38}Ar age for the larger sample is nominally somewhat higher at 11.0 ± 2.7 Myr, it is still consistent with the other ages within uncertainty. Cosmogenic ^{38}Ar tends to show larger variations due to the larger heterogeneity of its major target elements Ca, Fe, and K in ordinary chondrites (Di Gregorio et al., 2019). Using the correlations between ^{3}He, ^{21}Ne, and ^{26}Al production rates from the model of Leya and Masarik (2009), applied to a sample with a ^{26}Al production rate of 52 dpm/kg, we can derive ^{3}He and ^{21}Ne production rates for Dingle Dell, which yield slightly higher CRE ages of 9.0 and 9.4 Myr, respectively. All five ages combine to a CRE age of 9.32 ± 1.3 Myr. Dingle Dell falls close to a small peak in the CRE age histogram of the L chondrites that is centered at ~10 Myr (Marti & Graf, 1992). The consistency of the He and Ne ages also suggests that Dingle Dell did not lose cosmogenic He during or after its exposure to cosmic rays.

After subtraction of the cosmogenic component for He (with $^{4}He_{cos}/^{3}He_{cos} = 4.1$, based on Dalcher et al., 2013), and a trapped Ar component conservatively assumed to be fully atmospheric for Ar (with $^{40}Ar_{air}/^{36}Ar_{air} = 300$) which would contribute 4.4% to the measured ^{40}Ar for the larger sample, the remaining ^{4}He and ^{40}Ar can be assumed to be completely

TABLE 4. Abundances of 49 elements in the Dingle Dell ordinary chondrite analyzed by ICPMS.

Element	Unit	Dingle Dell abundance	Error (% RSD)	L chondrite abundance	LL chondrite abundance
Li	μg/g	1.7	5	1.9	2.0
Na	mg/g	8.3	4	6.9	6.9
Mg	mg/g	162	2	148	153
Al	mg/g	12.8	5	11.7	11.8
Sc	μg/g	9.1	11	8.4	8.3
Ti	μg/g	550	9	690	680
Mn	mg/g	2.71	2	2.58	2.6
Fe	mg/g	219	11	218	198
Co	μg/g	535	29	600	480
Ni	mg/g	12.7	26	12.7	10.2
Cu	μg/g	91	19	95	83
Zn	μg/g	59	16	54	55
Ga	μg/g	4.8	2	5.4	5.2
As	μg/g	1.0	9	1.4	1.3
Se	μg/g	8.4	20	9.2	9.1
Rb	μg/g	2.6	6	2.8	2.7
Sr	μg/g	8.6	7	11	11
Y	μg/g	2.3	14	2.1	2
Zr	μg/g	7.9	13	5.8	9.8
Nb	ng/g	490	7	400	400
Ru	ng/g	800	62	750	550
Pd	ng/g	720	17	620	510
Ag	ng/g	58	14	80	65
Sn	ng/g	340	28	400	330
Sb	ng/g	30	18	70	70
Te	ng/g	430	18	400	390
Cs	ng/g	11	10	200	170
Ba	μg/g	3.2	7	3.8	4
La	ng/g	300	19	330	330
Ce	ng/g	800	19	860	880
Pr	ng/g	120	18	130	130
Nd	ng/g	580	18	670	650
Sm	ng/g	200	16	203	210
Eu	ng/g	78	7	79	80
Gd	ng/g	280	16	300	290
Tb	ng/g	54	15	54	55
Dy	ng/g	290	14	360	350
Ho	ng/g	74	14	77	79
Er	ng/g	220	14	230	230
Tm	ng/g	36	13	33	35
Yb	ng/g	220	11	226	230
Lu	ng/g	40	11	34	34
Hf	ng/g	170	11	170	170
W	ng/g	110	17	150	100
Re	ng/g	50	19	55	32
Ir	ng/g	490	14	520	360
Pt	ng/g	930	7	1080	880
Th	ng/g	45	28	40	46
U	ng/g	12	47	13	13

Note: Mean abundances and errors based on the analysis of five replicate chips (see text). L and LL chondrite abundances from Lodders (2021).

radiogenic; we calculate nominal U, Th-He ages of 2.1 and 1.9 Gyr (for the larger and smaller samples, respectively) and a K-Ar age of 4.5 Gyr for the large sample using typical LL chondritic abundances for U, Th, and K (Wasson & Kallemeyn, 1988). We used LL chondritic abundances rather than L values since the

TABLE 5. Chemical composition of Dingle Dell chondrite based on ICP-OES measurements of the metal and stone fractions of Dingle Dell that were dissolved for cosmogenic radionuclides.

	Dingle Dell			L	LL
Element	Metal	Stone	Bulk	Bulk	Bulk
Mg	0.029	16.0	14.9	14.9	15.3
Al	–	1.21	1.13	1.22	1.19
P	–	0.13	0.12	0.095	0.085
S	–	3.0	2.8	2.2	2.3
K	–	0.111	0.103	0.082	0.079
Ca	–	1.33	1.24	1.31	1.30
Ti	–	0.065	0.061	0.063	0.062
Mn	–	0.26	0.24	0.26	0.26
Fe	83.5	18.1	22.5	21.5	18.5
Ni	14.0	0.39	1.30	1.20	1.02
Co (ppm)	6900	130	580	590	490
Sr (ppm)	–	11.0	10.3	11.1	11.1
Ba (ppm)	–	5.0	4.6	3.7	4.8

Note: The bulk composition of Dingle Dell is calculated from metal and stone composition, adopting 6.7 wt% metal and 93.3 wt% stone. All values are in wt%, except Co, Sr, and Ba, which are in ppm. Bulk values for average L and LL chondrite are from Wasson and Kallemeyn (1988).

ICP-MS results are more reflective of LL bulk chemistry, even though the meteorite is classified as an L.

DISCUSSION

Reclassification

Dingle Dell was originally classified as an LL6 chondrite in the 106th Meteoritical Bulletin (Gattacceca et al., 2019). This conclusion was primarily based on EPMA measurements of the silicate minerals (which showed values between L and LL, though closer to L), and the O-isotope compositions (more consistent with an LL chondrite). For this study, we re-measured the silicate mineral compositions and included measurements of kamacite, taenite, and chromite grains to yield the following values: olivine (Fa = 24.4 ± 0.3 mol%), pyroxene (Fs = 20.5 ± 0.2 mol%; Wo = 1.6 ± 0.3 mol%), kamacite (Ni = 6.43 ± 0.30 wt%; Co = 0.99 ± 0.22 wt%), and chromite (2.84 ± 0.23 wt%) (Figure 8). Although Benedix et al. (2017) report higher Fa (25.5 ± 0.4) and Fs (21.9 ± 0.2) values which more closely resemble an intermediate L/LL class, their analysis did not include metal or chromite grains. Since all these mineral compositions are the traditionally accepted method for chondrite classification (Kallemeyn et al., 1989; Rubin, 1990; Scott et al., 1986), and our measurements show L chondrite compositions across all mineral types (silicates, metals, and oxides), we revise the classification of Dingle Dell to an L chondrite. Although oxygen isotopes are often used to distinguish between different meteorite classes, recent analysis by Kirby et al. (2025) demonstrates that considerable overlap between L and LL chondrites exists with respect to this characteristic, while also reinforcing the reliability of mineral chemistry as a class indicator. Given that Dingle Dell's mineral chemistry clearly indicates an L chondrite class, while the oxygen isotope compositions are on the border between L and LL, we defer to mineral compositions as the deciding factor in Dingle Dell's classification. As some chondrules are identifiable in the μCT scans, the SEM-EDS images, and the thin sections which resemble a petrologic type 6 chondrite, we therefore fully reclassify Dingle Dell as an L6 chondrite.

Despite the reclassification, many of Dingle Dell's other characteristics include both L and LL features, depending on the feature in question. Dingle Dell's oxygen isotope compositions are within the expected value range for LL chondrites, though they are near the L/LL border (Figure 12). The Cr isotope composition of this meteorite (Figure 10) is typical for both L and LL chondrites. The bulk elemental composition determined from five chips of Dingle Dell via ICPMS fits best into the LL group (Figure 9, Table 4), although some siderophile elemental abundances asre closer to the L group. Meanwhile, ICP-OES results show metal phase compositions consistent with an L chondrite. Normally, this cm-scale variation is associated with brecciation, but neither the μCT scans nor the thin sections reveal heterogeneity or textures to support this. In the future, multi-methodology studies of meteorites such as they may benefit from characterization of multiple pieces of the same meteorite to quantify the limits of compositional variability within a single meteorite.

Dingle Dell's bulk and grain densities are typical for both L and LL chondrites (Britt & Consolmagno, 2003; Macke, 2010), while the porosity is also reasonable for a mildly shocked, equilibrated ordinary chondrite (Friedrich et al., 2017). The magnetic susceptibility for Dingle Dell is most comfortably grouped with L chondrites, although it is also near the border for the expected values of the LL group (Consolmagno et al., 2006; Macke, 2010).

Amino Acid Contamination

The speedy recovery of the main mass prior to experiencing rainfall prevented any detectable mineral weathering from taking place. Nevertheless, this week-long stay at the fall location was long enough to contaminate the meteorite with terrestrial amino acids. Although extraterrestrial amino acids could

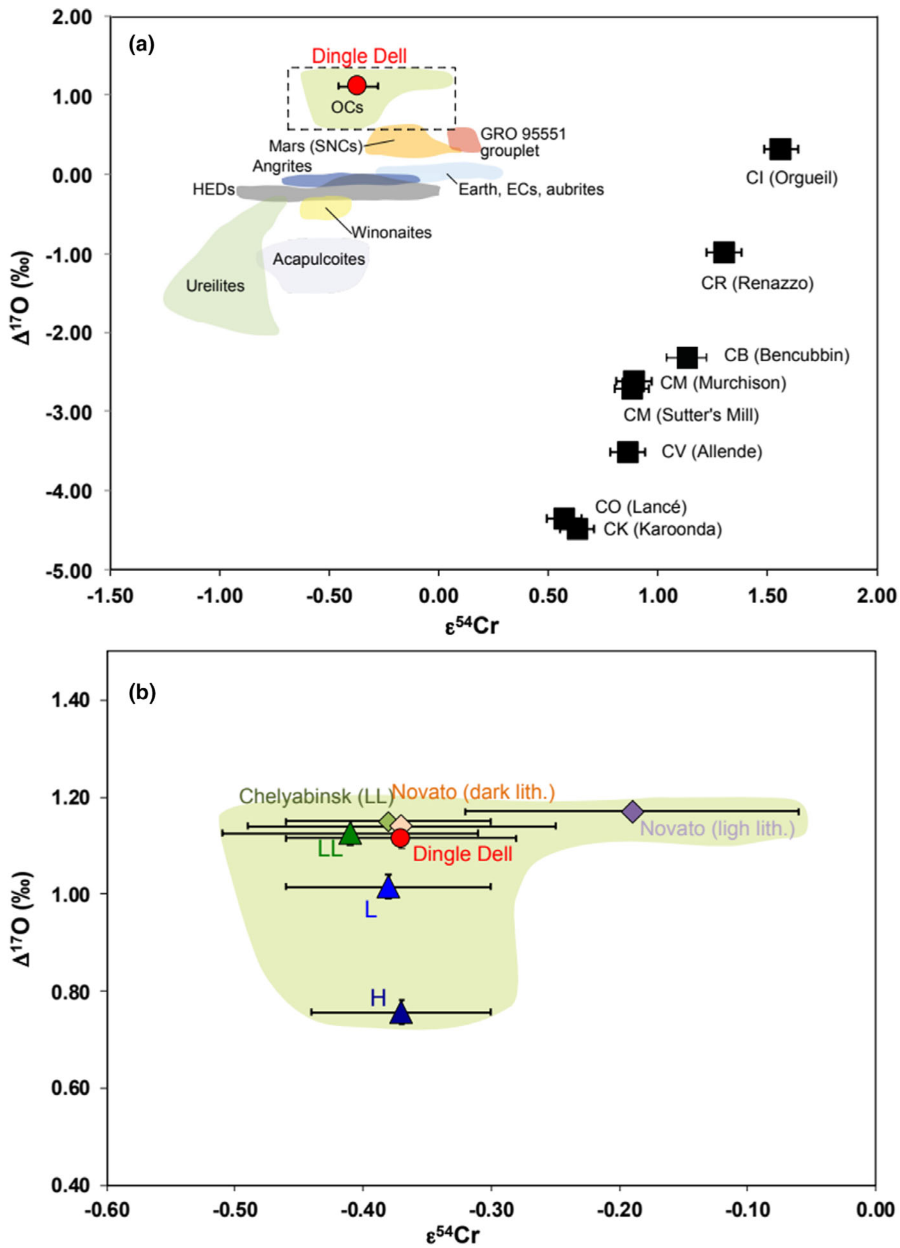

FIGURE 10. (a) ε^{54}Cr versus Δ^{17}O plot of Dingle Dell (red circle) in relation to achondrites, ordinary chondrites, enstatite chondrites, carbonaceous chondrites (black squares), and Earth (light blue shaded region). (b) ε^{54}Cr versus Δ^{17}O plot of Dingle Dell (red circle) focused in on the area defined by ordinary chondrites (beige shaded region)—indicated by dashed box in panel (a). Average compositions of H, L, and LL chondrites (triangles) and individual ordinary chondrites (diamonds) are also plotted. Literature data for Δ^{17}O are from Clayton and Mayeda (1988, 1996, 1999); Clayton et al. (1984, 1991); Jenniskens et al. (2012, 2014); Li et al. (2018); Popova et al. (2013); Rubin et al. (2002); Scott et al. (2009). Literature data for ε^{54}Cr are from Jenniskens et al. (2012, 2014); Li et al. (2018); Popova et al. (2013); Shukolyukov and Lugmair (2006); Trinquier et al. (2007); Ueda et al. (2006).

conceivably be present within Dingle Dell, distinguishing them from the terrestrial component is not possible without consuming the many grams of sample required for compound-specific stable isotope analyses. Amino acid studies of other L or LL ordinary chondrites are rare. The Novato L6 ordinary chondrite (Jenniskens et al., 2014) which also has a characterized orbit, and was also recovered prior to rain fall, showed evidence of contamination based on enantiomeric ratios and distributions as well, though no soil was available for a direct comparison. The Çanakkale L6 ordinary chondrite was recovered after a fall in 1964, the

TABLE 6. Chromium isotopic composition of Dingle Dell and other ordinary chondrites (2σ uncertainties).

	Type	ε^{53}Cr	ε^{54}Cr
Dingle Dell	L6	0.20 ± 0.04	−0.37 ± 0.09
Novato (dark)	L6	0.23 ± 0.04	−0.37 ± 0.12
Novato (light)	L6	0.20 ± 0.04	−0.19 ± 0.13
Chainpur	L3.4	0.24 ± 0.06	−0.47 ± 0.07
Chelyabinsk	LL5	0.23 ± 0.03	−0.38 ± 0.08
Olivenza	LL5	0.23 ± 0.06	No data
Saint-Séverin	LL6	0.28 ± 0.06	−0.41 ± 0.10
Knyahinya	L5	0.15 ± 0.06	−0.38 ± 0.08
Ste.-Marguerite	H4	0.13 ± 0.06	−0.39 ± 0.07
Kernouvé	H6	0.19 ± 0.06	−0.37 ± 0.07

Note: Cr data references: Novato—Jenniskens et al. (2014), Chainpur, Saint- Séverin, Knyahinya, Ste.-Marguerite, Kernouvé—(Trinquier et al., 2007, 2008), Chelyabinsk—(Popova et al., 2013).

fragments studied were discovered to have been stored loose in a desk drawer in the Department of Astronomy, Istanbul University in the office of a tobacco smoker from 1964 to 2007 (C.Y. Ornek personal communication) and unsurprisingly showed amino acid contamination consistent with soil and/or plausible combustion products (Burton et al., 2016). The Shişr 031 and 035 L6 ordinary chondrites (Martins et al., 2007) have terrestrial ages of 15.0 ± 0.4 ka and 21.4 ± 1.3 ka, respectively, but were collected in an arid desert in Oman followed by prompt analysis. The amino acid abundance of these L6 chondrites is low and can also be explained by contamination. The Antarctic LL5 ordinary chondrites La Paz Icefields 03784, 03573, 03624, and 16154 also show very low levels of amino acids that are mostly attributed to contamination from the Antarctic ice which they were in direct contact with for perhaps 13,000 years (Botta et al., 2008). Thus, even with prompt collection after a fall in an arid environment, as was the case with Dingle Dell, terrestrial amino acid contamination from the landing site is rapid and can overprint any extraterrestrial amino acids in organic-poor meteorites and even be problematic for some fragments of organic-rich meteorites which fell in tropical regions like Aguas Zarcas (Glavin et al., 2021). Thus, to confirm the presence of any extraterrestrial amino acids in thermally altered L or LL ordinary chondrites like Dingle Dell that are likely amino acid depleted, the analysis of pristine materials from sample return that have not experienced any exposure to the terrestrial environment may be required.

Meteoritic Siblings and Asteroid Origin

Linking Dingle Dell to other photographically observed L and LL meteorite falls is not immediately obvious. This is partially due to the incomplete CRE age and source region information for all of these samples (see Table 11; Granvik & Brown, 2018; Jenniskens & Devillepoix, 2025; Meier, 2024; https://www.meteoriteorbits.info, accessed April 2026). For meteorites with known prior orbits to be closely associated, they should have similar CRE ages, mineral compositions, source regions, and impact histories, or at least some combination of those features. Since Dingle Dell was delivered to the Earth from the main asteroid belt with low inclination (Devillepoix et al., 2018), we will narrow our comparison to other meteorites that also come from the main asteroid belt ($a > \sim1.5$ AU) with low inclination ($i < 10°$). The L and LL chondrites that fit these criteria are listed in Table 11.

To properly compare the orbits of these meteorites with the intent of identifying "meteoritic siblings" to Dingle Dell, we must first consider how meteorites are delivered from asteroids to Earth, beginning with an ejection event on the meteorite's contemporary source body: the asteroid that exists in present day, or at least existed at the time of ejection, not the parent body that formed in the early solar system which accreted material and was subjected to metamorphism to create the meteorite's type and class. Once a smaller (meter-sized) object is ejected from its asteroid, it is bombarded by galactic and solar cosmic rays until it lands on the surface of the Earth, assuming it was not already on the surface of its source body. Meteorites that were exposed to cosmic rays on the surface of the parent body before ejection are known to have a complex CRE history, while the majority of meteorites, such as Dingle Dell, that were only exposure to cosmic rays as a small object in space are known to have a simple CRE history.

In the latter case, for known falls, the CRE age directly corresponds to the transfer time from the parent body to Earth. The length of this bombardment can be quantified by a number of mass spectrometry techniques coupled with numerical modeling (see methods section); for Dingle Dell, this Cosmic Ray Exposure (CRE) Age is placed at 9.3 ± 1.3 Myr. Over the course of these millions of years, the Yarkovsky effect (Bottke Jr et al., 2006) begins to increase or decrease the semimajor axis of the meteoroid, depending on the direction of its spin, until it crosses into an orbital resonance with either Saturn or, more commonly, Jupiter, which then increases the meteoroid's inclination or eccentricity, respectively. This eventually causes the meteoroid to impact an inner planet or be ejected out of the solar system, via close encounter.

Orbital modeling (Devillepoix et al., 2018) shows that Dingle Dell had a pre-impact semimajor axis of 2.254 AU and was delivered to the Earth via the 3:1 mean motion resonance with Jupiter. If a sibling

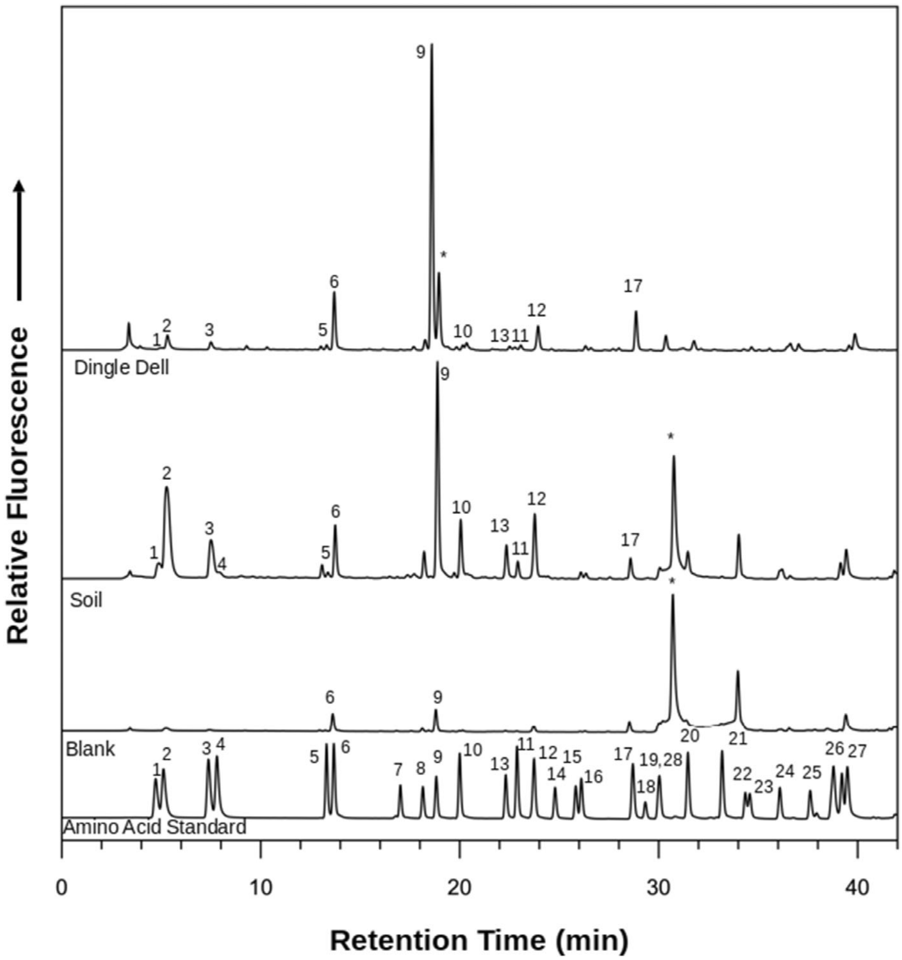

FIGURE 11. The hot water extracts for the procedural blank, soil, standard, and the Dingle Dell meteorite are shown. Peaks were identified by comparison of the procedural blank or sample UV fluorescence retention times and m/z values to those peaks in the amino acid standard analyzed on the same day and are designated by peak number as follows: (1) D-aspartic acid; (2) L-aspartic acid; (3) L-glutamic acid; (4) D-glutamic acid; (5) D-serine; (6) L-serine; (7) D-threonine; (8) L-threonine; (9) glycine; (10) b-alanine; (11) D-alanine; (12) L-alanine; (13) γ-amino-n-butyric acid + D,L-b-aminoisobutyric acid; (14) D-b-amino-n-butyric acid; (15) L-b-amino-n-butyric acid; (16) a-aminoisobutyric acid; (17) D,L-a-amino-n-butyric acid; (18) D-isovaline; (19) L-isovaline; (20) L-valine; (21) D-valine; (22) D-norvaline; (23) L-norvaline; (24) L-leucine; (25) D-leucine; (26, 27) D,L-isoleucine; and (28) e-amino-n-caproic acid. The peak labeled "*" is a desalting artifact, and the peak labeled "x" is an unidentified workup or an analytical artifact.

meteoroid was ejected from the same contemporary source body but with an opposite spin, it is conceivable that the Yarkovsky effect would cause an inward migration toward the ν_6 secular resonance. When we also consider CRE ages (where they are available, see Table 11), the only obvious connection to Dingle Dell (9.3 ± 1.3 Myr) meteorite is Novato (L6 chondrite; 9 ± 1 Myr; Jenniskens et al., 2014). This assumes that this co-ejection occurred between the ν_6 and 3:1 resonances but resulted in opposite spins for the two meteoroids, sending them outward (Dingle Dell) and inward (Novato) in the solar system. While dynamically this is plausible, Novato is a brecciated L6 chondrite that exhibits signs of notably more intense shock pressure (S4) in its history than Dingle Dell and likely belongs to the group of shocked L chondrites with shock ages near 470 Myr (Korochantseva et al., 2007; Weirich et al., 2012), making a connection based on their physical nature difficult. Another conceivable scenario envisions multiple ejections separated by millions of years from the same source body, sending meteoroids toward the 3:1 and ν_6 resonances, which could make most of the meteorites listed in Table 11 related to Dingle Dell in some way. It is also entirely possible that each of those meteorites was ejected from separate source bodies and are not related to each other.

TABLE 7. Comparison of the D/L ratios measured for several amino acids measured in the water extracts of the Dingle Dell meteorite and soil collected from the meteorite fall site.

	Dingle Dell				Soil (Al Foil)			
	Free		Total		Free		Total	
Amino acids	D/L	L_{ee} (%)	D/L	L_{ee} (%)	D/L	L_{ee} (%)	D/L	L_{ee} (%)
Aspartic acid	0.29 ± 0.02	55 ± 2	0.17 ± 0.01	70 ± 1	0.19 ± 0.01	68 ± 1	0.35 ± 0.02	48 ± 2
Glutamic acid	0.09 ± 0.01	84 ± 1	0.10 ± 0.01	83 ± 1	0.12 ± 0.01	79 ± 1	0.24 ± 0.03	62 ± 3
Serine	0.11 ± 0.01	84 ± 1	0.05 ± 0.01	83 ± 1	0.08 ± 0.01	68 ± 1	0.33 ± 0.04	88 ± 1
Alanine	0.35 ± 0.01	49 ± 1	0.12 ± 0.01	79 ± 1	0.38 ± 0.03	45 ± 2	0.16 ± 0.01	73 ± 1
β-Amino-*n*-butyric acid	n.d.	n.d.	n.d.	n.d.	0.08 ± 0.01	85 ± 1	n.d.	n.d.
Isovaline	n.d.	n.d.	n.d.	n.d.	n.d.	n.d.	n.d.	n.d.
Valine	n.d.	n.d.	n.d.	n.d.	n.d.	n.d.	n.d.	99 ± 1

Note: n.d. = value not determined due to trace amino acid concentrations or analytical interferences. %Lee = ([L-D]/[L + D]) × 100.

TABLE 8. Summary of the average concentrations of free and total amino acids in the hot water extracts of the Dingle Dell meteorite and soil collected from the meteorite fall site.[a]

	Dingle Dell meteorite		Fall site soil	
Amino acid	Free	Total	Free	Total
Dicarboxylic amino acids				
D-Aspartic acid	<0.01	0.035 ± 0.001	<0.01	2.220 ± 0.089
L-Aspartic acid	0.010 ± 0.001	0.203 ± 0.003	0.340 ± 0.015	6.260 ± 0.310
L-Glutamic acid	0.035 ± 0.002	0.302 ± 0.004	1.537 ± 0.088	6.319 ± 0.389
D-Glutamic acid	0.019 ± 0.001	0.029 ± 0.002	0.490 ± 0.026	1.501 ± 0.160
Hydroxy amino acids				
D-Serine	<0.01	0.028 ± 0.001	0.077 ± 0.010	0.238 ± 0.023
L-Serine	0.012 ± 0.001	0.533 ± 0.005	0.071 ± 0.005	3.664 ± 0.180
D-Threonine	0.103 ± 0.003	0.287 ± 0.017	0.400 ± 0.031	8.514 ± 0.488
L-Threonine	<0.01	4.668 ± 0.064	<0.01	3.024 ± 0.228
C_2 amino acid				
Glycine	0.677 ± 0.192	1.212 ± 0.027	3.667 ± 0.402	44.625 ± 5.002
C_3 amino acids				
β-Alanine	0.025 ± 0.001	0.154 ± 0.006	0.622 ± 0.040	4.434 ± 0.238
D-Alanine	0.013 ± 0.001	0.030 ± 0.001	0.156 ± 0.016	1.755 ± 0.059
L-Alanine	0.037 ± 0.001	0.248 ± 0.004	0.478 ± 0.024	11.194 ± 0.452
C_4 amino acids				
ɣ-Amino-*n*-butyric acid (ɣ-ABA)	0.012 ± 0.001	0.177 ± 0.004	0.312 ± 0.105	1.566 ± 0.084
D-β-Amino-*n*-butyric acid (D-β-ABA)	<0.01	<0.01	<0.01	<0.01
L-β-Amino-*n*-butyric acid (L-β-ABA)	0.030 ± 0.001	<0.01	0.130 ± 0.010	0.021 ± 0.003
α-Aminoisobutyric acid (α-AIB)	<0.01	0.044 ± 0.000	0.126 ± 0.005	0.054 ± 0.005
D + L-α-Amino-*n*-butyric acid[b] (α-ABA)	<0.01	<0.01	<0.01	<0.01
C_5 amino acids				
D-Isovaline	<0.01	<0.01	<0.01	<0.01
L-Isovaline	<0.01	<0.01	<0.01	<0.01
L-Valine	<0.01	0.093 ± 0.002	0.108 ± 0.008	11.242 ± 0.754
D-Valine	<0.01	<0.01	<0.01	0.052 ± 0.003
C_6 amino acids				
ε-Amino-*n*-caproic acid	0.033 ± 0.039	0.149 ± 0.009	0.143 ± 0.129	0.065 ± 0.145

[a]Values are reported in nmol/g based on the bulk sample mass. Sample extracts were analyzed by OPA/NAC derivatization (15 min) and LC separation with UV fluorescence and time of flight. For the LC/ToF-MS data, the mono-isotopic masses of each protonated OPA/NAC were used for quantification. Amino acid concentrations were determined from both UV fluorescence and single ion mass peak areas and included background level correction using a procedural blank and comparison of the peak areas with those of an amino acid standard run on the same day. The reported uncertainties (δx) are based on the standard deviation of the average value of multiple individual measurements (n), where $\delta x = \sigma x$ (n)–1/2. For all UV fluorescence data, coeluting peaks and/or compounds with interfering peaks were not included in the average. Upper limits are presented for amino acids that were not present at levels above the procedural blank background levels.

[b]Enantiomers could not be separated under the chromatographic conditions.

TABLE 9. Cosmogenic radionuclide concentrations (listed in disintegrations per minute per kg (dpm kg^{-1}); 1σ uncertainties) in the stone and metal fractions of Dingle Dell.

Phase	Mass (mg)	^{10}Be	^{26}Al	^{36}Cl
Stone	91.0	19.5 ± 0.2	55.7 ± 1.3	7.26 ± 0.09
Metal	74.4	5.84 ± 0.11	4.16 ± 0.12	21.9 ± 0.6
Bulk	N/A	18.5 ± 0.2	52.2 ± 1.2	N/A

Note: Bulk values were calculated from measured radionuclide concentrations in the metal and stone fraction and metal content of 6.7 wt% in the bulk meteorite.

Linking Dingle Dell to contemporary asteroids or asteroid families is also somewhat nuanced. Nesvorný et al. (2009) propose a connection between many L chondrites and the Gefion family breakup, using the 5:2 resonance with Jupiter as the delivering mechanism, though this is at odds with Dingle Dell's proposed origin on the sunward side of the 3:1 resonance. Furthermore, Nesvorný et al. (2009) highlight the major breakup event recorded at ~470 Ma in many L chondrites as the key evidence to link them to the dynamical dispersions observed in the Gefion family.

TABLE 10. Measured noble gas concentrations for Dingle Dell, reported in 10^{-8} cm^3 STP g^{-1}.

Sample mass	^{3}He	^{4}He	^{20}Ne	^{21}Ne	^{22}Ne	^{36}Ar	^{38}Ar	^{40}Ar	$^{40}Ar/^{36}Ar$
37.1 mg	15.1	740	2.41	2.41	2.80	1.18	0.58	6200	5260
27.1 mg	15.3	679	2.44	2.40	2.81	n.d.	n.d.	6530	n.d.

Note: Typical uncertainties are 3%.

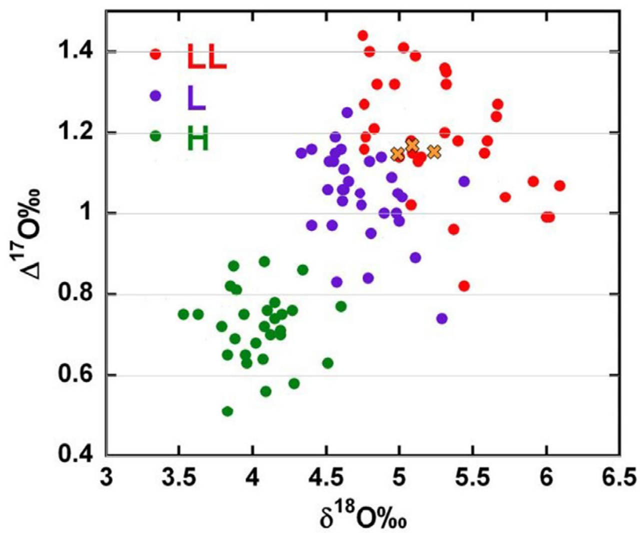

FIGURE 12. Oxygen isotope ratios for Dingle Dell (appearing as yellow X's), plotted against values for H, L, and LL chondrites. Data for other ordinary chondrites taken from Clayton et al. (1991).

Since this ~470 Ma pressure–temperature event is not recorded in our analyses, and considering that their orbital delivery pathways are dissimilar, we do not suggest that Dingle Dell originated from the Gefion Family. While the Flora family is often identified as a possible progenitor of LL chondrites (Vernazza et al., 2008), it sends meteorites from the asteroid belt to an Earth-crossing orbit via the ν_6 secular resonance, which is only 12% likely to be the source region for Dingle Dell (Devillepoix et al., 2018). Although recent work by Marsset et al. (2024) argues that the Massalia asteroid family could be a source for L chondrites being delivered via the 3:1 resonance, much of their argument focuses on the connection between the <500 Myr collisional breakup of the family and the ~470 Myr impact event recorded in many L chondrites, an event that is absent in Dingle Dell's history. A meta-study by Jenniskens and Devillepoix (2025) that compared meteorites with known orbits to possible asteroidal sources suggests that the Hertha asteroid family could instead be responsible for the delivery of many L chondrites to the Earth. They suggest that a source asteroid or family is delivering L chondrites from the inner Main Belt between the 3:1 and ν_6 resonances with multiple ejection events, one of which may have occurred ~9 Ma, due to the clustering of other L chondrite CRE ages. This closely aligns with Dingle Dell's prior orbit and CRE age. Although notably, Jenniskens and Devillepoix (2025) posit that the ~470 Ma impact event in the meteoritic record is not distinguishable from a dynamics perspective and suggest that two meteorites that have dissimilar shock-impact chronologies could still be associated with the same asteroid family, and therefore, discounting a connection due to a lack of shared gas retention chronology is not valid in isolation. This means that we cannot discount or confirm either the Hertha or Massalia asteroid families as Dingle Dell's source in the solar system. As more meteorites with known orbits are recovered and characterized, we can more robustly group Dingle Dell together with other L chondrites originating from a low-inclination source in the inner Main Belt.

CONCLUSIONS

The Dingle Dell L6 orbital meteorite is an unshocked, unweathered, unbrecciated, equilibrated ordinary chondrite from the inner main asteroid belt that compositionally resides near the border between the L and LL chondrite groups (main features listed in Table 12). Its gas retention ages do not show evidence of the impact event ~470 Ma associated with many L chondrites. The CRE age of 9.3 Myr overlaps with a cluster at 10 Myr in the L-chondrite ages (Marti & Graf, 1992), though this peak is dominated by shocked L chondrites that lost most of their radiogenic gases in a major impact event, unlike Dingle Dell. Orbital modeling of Dingle Dell's meteoroid does not clearly indicate an origin in either the Flora or Gefion asteroid families, the theorized source of many L and LL chondrites, respectively. Although the Hertha and Massalia asteroid families are each theorized to source L chondrites to the Earth from the inner main asteroid belt, as of yet, we cannot determine which family is the most likely progenitor. Its relation to other L and LL chondrite falls with recorded orbits is also not obvious, though Novato (L6, brecciated) shows the most promise as a meteoritic sibling. Dingle Dell's mostly L-like, but sometimes LL-like features may indicate that future systematic work is

TABLE 11. L and LL chondrites delivered by orbits from the main asteroid belt with low inclination and others that may be related to Dingle Dell (appearing in bold).

Name	Type	*a* (AU)	*E*	*i* (°)	Arg Peri (°)	Asc Node (°)	CRE (Ma)	Refs.	Source Region
Dingle Dell	**L6**	**2.254 ± 0.034**	**0.590 ± 0.006**	**4.051 ± 0.012**	**215.773 ± 0.049**	**218.252 ± 0.000**	**9.3 ± 1.3**	**a**	**3:1J**
Park Forest	L5	2.53 ± 0.21	0.680 ± 0.025	3.25 ± 0.66	237.5 ± 2.0	6.1153 ± 0.0003	14 ± 2	b	3:1J
Villalbeto de la Peña	L6	2.30 ± 0.22	0.627 ± 0.036	0.02 ± 0.49	134 ± 180	282 ± 180	48 ± 5	c	*ν*6
Novato	L6	2.091 ± 0.079	0.528 ± 0.018	5.52 ± 0.11	347.36 ± 0.30	24.9625 ± 0.0002	9 ± 1	d	*ν*6
Porangaba	L4	2.54 ± 1.1	0.64 ± 0.11	8.6 ± 3.2	142.8 ± 6.7	288.921 ± 0.001	–	e	3:1J
Kindberg	L6	2	0.533	5	205.5	237	–	f	–
Innisfree	L5	1.866 ± 0.051	0.472 ± 0.014	12.250 ± 0.22	177.97 ± 0.13	317.5223 ± 0.0002	26–28	g	*ν*6
Žd'ár nad Sázavou	L3	2.1020 ± 0.0088	0.6808 ± 0.0015	2.809 ± 0.018	257.748 ± 0.043	257.2618 ± 0.0002	–	h	*ν*6
Benešov	LL3.5, H5	2.4826 ± 0.0024	0.6273 ± 0.0004	23.9807 ± 0.0074	218.369 ± 0.017	47.0004 ± 0.0000	–	i	3:1J
Jesenice	L6	1.744 ± 0.068	0.429 ± 0.023	9.58 ± 0.48	190.49 ± 0.54	19.1950 ± 0.0002	~4	j	*ν*6
Novo Mesto	L5	1.451 ± 0.004	0.60866 ± 0.0006	8.755 ± 0.063	82.649 ± 0.184	338.9930	–	k	–
Cavezzo	L5-an	1.82 ± 0.22	0.460 ± 0.063	4.0 ± 1.6	179.2 ± 4.8	280.52311 ± 0.00001	-	l	–
Osceola	L6	1.486	0.3406	13.20	169.0	303.9	18 ± 2	m	–
Chelyabinsk	LL5	1.770 ± 0.022	0.5792 ± 0.0061	4.78 ± 0.13	109.22 ± 0.18	326.4136 ± 0.0003	1	n	*ν*6
Stubenburg	LL6	1.525 ± 0.010	0.395 ± 0.004	2.07 ± 0.03	221.02 ± 0.03	346.5197	36 ± 3	o	–

Note: All orbital data for other meteorites are sourced from Granvik and Brown (2018), excluding Porangaba, Cavezzo, Osceola, Stubenburg, and Kindberg (see references below). (a) Devillepoix et al. (2018); (b) Brown et al. (2004), Simon et al. (2004), Meier et al. (2017); (c) Llorca et al. (2005); (d) Jenniskens et al. (2014); (e) Ferus et al. (2020); (f) Kővágó (2021); (g) Halliday et al. (1978), Goswami et al. (1978); (h) Spurný et al. (2020); (i) Spurný et al. (2014); (j) Bischoff et al. (2011); (k) Vida et al. (2021); (l) Pratesi et al. (2021), Gardiol et al. (2021); (m) Meier et al. (2020), Bouvier et al. (2017); (n) Righter et al. (2015), Borovička et al. (2013); (o) Bischoff et al. (2017), Spurny et al. (2016).

TABLE 12. Major features of the Dingle Dell L6 chondrite.

Feature	Result	Method
Class	L6	Optical microscopy
	L6	SEM
	L5-6	EPMA
	LL	Oxygen isotope analysis
	L or LL	ICPMS
	LL	XRD
Shock state	S2	Optical microscopy
Weathering grade	W0	Visual inspection
Oxygen isotope ratios	$\delta^{17}O = 3.809 \pm 0.068$ $\delta^{18}O = 5.102 \pm 0.126$ $\Delta^{17}O = 1.115 \pm 0.011$	Laser-assisted fluorination ($n = 3$)
Chromium isotope anomaly	$\varepsilon^{54}Cr = -0.37 \pm 0.09$	TIMS ($n = 4$)
Cosmic ray exposure age	9.3 ± 1.3 Myr	Combined noble gas and radionuclide accelerator mass spectrometry analyses
Meteoroid size (radius)	14–18 cm	Fireball observations
	10–15 cm	Noble gas concentrations
Mineral chemistry	$Fa_{25.1\pm0.4}$ ($n = 21$) $Fs_{21.2\pm0.2}$ ($n = 22$) $Wo_{1.3\pm0.1}$ ($n = 22$)	EPMA
Porosity	$10.5 \pm 0.5\%$	He pycnometry
Grain density	3.61 ± 0.01 g cm^{-3}	He pycnometry
	3.45 g cm^{-3}	Coarse CT
Bulk density	3.23 ± 0.02 g cm^{-3}	He pycnometry
Magnetic susceptibility	Log $\chi = 4.78 \pm 0.09$	Magnetic susceptibility probe
Chondrule diameter	0.9 ± 0.5 mm ($n = 15$)	SEM

Note: All uncertainties reported are 1σ, except ε^{54}Cr, which is 2σ.

needed to properly characterize the limits of the overlap between L and LL chondrites. Finally, despite Dingle Dell's comparatively speedy recovery prior to any significant exposure to terrestrial sources of water and other organics, its extraterrestrial organic inventory is completely contaminated with terrestrial sources, highlighting the unique advantage offered by asteroid sample return missions.

Acknowledgments—This work was funded by Australian Research Council's Discovery Project (DP200102073). This work was supported by a NASA Postdoctoral Program Fellowship administered by Oak Ridge Associated Universities. This research was supported in part by the NASA Astrobiology Institute through funding awarded to the Goddard Center for Astrobiology under proposal 13-13NAI7-0032 for lab support and a fellowship for K.M.Y. and by a grant from the Simons Foundation (SCOL award 302497 to J.P.D.); The material is based upon in part on work supported by NASA under award number 80GSFC21M0002 for H.L.M. This work has been carried out in parts within the framework of the NCCR PlanetS supported by the Swiss National Science Foundation under grants 51NF40 182901 and 51NF40 205606 and was supported by a Swiss National Science Foundation "Ambizione" grant to M.M (PZ00P2 154874). The authors acknowledge support from UKRI STFC grants (ST/Y004817/1, ST/T002328/1, and ST/W001128/1).

Conflict of Interest Statement—The authors declare no conflict of interest in publishing this paper.

Data Availability Statement—The data that support the findings of this study are available from the corresponding author upon reasonable request.

REFERENCES

Afiattalab, F., and Wasson, J. T. 1980. Composition of the Metal Phases in Ordinary Chondrites: Implications Regarding Classification and Metamorphism. *Geochimica et Cosmochimica Acta* 44: 431–446.

Anderson, S. 2023. Farm to Table Meteorites: An End to End Exploration of the Solar System's Past, Present, and Future, Doctoral dissertation, Curtin University, Perth, Western Australia. https://espace.curtin.edu.au/handle/20.500.11937/92481.

Benedix, G. K., Forman, L. V., Daly, L., Godel, B., Esetban, L., Meier, M. M. M., Maden, C., et al. 2017. Mineralogy, Petrology and Chronology of the Dingle Dell Meteorite. *80th Annual Meeting of the Meteoritical Society 2017*.

Bischoff, A., Barrat, J. A., Bauer, K., Burkhardt, C., Busemann, H., Ebert, S., Gonsior, M., et al. 2017. The Stubenberg Meteorite—An LL 6 Chondrite Fragmental Breccia Recovered Soon after Precise Prediction of the Strewn Field. *Meteoritics & Planetary Science* 52: 1683–1703.

Bischoff, A., Jersek, M., Grau, T., Mirtic, B., Ott, U., Kučera, J., Horstmann, M., et al. 2011. Jesenice—A New Meteorite Fall from Slovenia. *Meteoritics & Planetary Science* 46: 793–804.

Bland, P. A., Spurný, P., Bevan, A. W. R., Howard, K. T., Towner, M. C., Benedix, G. K., Greenwood, R. C., et al. 2012. The Australian Desert Fireball Network: A New Era for Planetary Science. *Australian Journal of Earth Sciences* 59: 177–187.

Borovička, J., Spurný, P., Brown, P., Wiegert, P., Kalenda, P., Clark, D., and Shrbený, L. 2013. The Trajectory, Structure and Origin of the Chelyabinsk Asteroidal Impactor. *Nature* 503: 235–37.

Botta, O., Martins, Z., Emmenegger, C., Dworkin, J. P., Glavin, D. P., Harvey, R. P., Zenobi, R., Bada, J. L., and Ehrenfreund, P. 2008. Polycyclic Aromatic Hydrocarbons and Amino Acids in Meteorites and Ice Samples from LaPaz Icefield, Antarctica. *Meteoritics & Planetary Science* 43: 1465–80.

Bottke, W. F., Jr., Vokrouhlický, D., Rubincam, D. P., and Nesvorný, D. 2006. The Yarkovsky and YORP Effects: Implications for Asteroid Dynamics. *Annual Review of Earth and Planetary Sciences* 34: 157–191.

Bouvier, A., Gattacceca, J., Grossman, J., and Metzler, K. 2017. The Meteoritical Bulletin, No. 105. *Meteoritics & Planetary Science* 52: 2411.

Britt, D. T., and Consolmagno, S. J. 2003. Stony Meteorite Porosities and Densities: A Review of the Data Through 2001. *Meteoritics & Planetary Science* 38: 1161–80.

Brown, P., Pack, D., Edwards, W. N., ReVelle, D. O., Yoo, B. B., Spalding, R. E., and Tagliaferri, E. 2004. The Orbit, Atmospheric Dynamics, and Initial Mass of the Park Forest Meteorite. *Meteoritics & Planetary Science* 39: 1781–96.

Brown, P. G., McCausland, P. J. A., Hildebrand, A. R., Hanton, L. T. J., Eckart, L. M., Busemann, H., Krietsch, D., et al. 2023. The Golden Meteorite Fall: Fireball Trajectory, Orbit, and Meteorite Characterization. *Meteoritics & Planetary Science* 58: 1773–1807.

Bunch, T. E., Keil, K., and Snetsinger, K. G. 1967. Chromite Composition in Relation to Chemistry and Texture of Ordinary Chondrites. *Geochimica et Cosmochimica Acta* 31: 1569–82.

Burton, A. S., Elsila, J. E., Callahan, M. P., Martin, M. G., Glavin, D. P., Johnson, N. M., and Dworkin, J. P. 2012. A Propensity for n-ω-Amino Acids in Thermally Altered Antarctic Meteorites. *Meteoritics & Planetary Science* 47: 374–386.

Burton, A. S., Elsila, J. E., Glavin, D. P., Dworkin, J. P., Ornek, C. Y., Esenoglu, H. H., Unsalan, O., and Ozturk, B. 2016. Searching for Extraterrestrial Amino Acids in a Contaminated Meteorite Amino Acid Analyses of the Çanakkale L6 Chondrite. *Lunar and Planetary Science Conference 2016*, abstract #2961.

Burton, A. S., McLain, H. L., Glavin, D. P., Elsila, J. P., Davidson, J., Miller, K. E., Andronikov, A. V., Lauretta, D., and Dworkin, J. P. 2015. Amino Acid Analyses of R and CK Chondrites. *Meteoritics & Planetary Science* 50: 470–482.

Busemann, H., Baur, H., and Wieler, R. 2000. Primordial Noble Gases in "Phase Q" in Carbonaceous and Ordinary Chondrites Studied by Closed-System Stepped Etching. *Meteoritics & Planetary Science* 35: 949–973.

Chan, H. S., Martins, Z., and Sephton, M. A. 2012. Amino Acid Analyses of Type 3 Chondrites Colony, Ornans, Chainpur, and Bishunpur. *Meteoritics & Planetary Science* 47: 1502–16.

Clayton, R. N., and Mayeda, T. K. 1988. Formation of Ureilites by Nebular Processes. *Geochimica et Cosmochimica Acta* 52: 1313–18.

Clayton, R. N., and Mayeda, T. K. 1996. Oxygen Isotope Studies of Achondrites. *Geochimica et Cosmochimica Acta* 60: 1999–2017.

Clayton, R. N., and Mayeda, T. K. 1999. Oxygen Isotope Studies of Carbonaceous Chondrites. *Geochimica et Cosmochimica Acta* 63: 2089–2104.

Clayton, R. N., Mayeda, T. K., Goswami, J. N., and Olsen, E. J. 1991. Oxygen Isotope Studies of Ordinary Chondrites. *Geochimica et Cosmochimica Acta* 55: 2317–37.

Clayton, R. N., Mayeda, T. K., and Rubin, A. E. 1984. Oxygen Isotopic Compositions of Enstatite Chondrites and Aubrites. *Journal of Geophysical Research* 89: C245–C249.

Consolmagno, G. J., Britt, D. T., and Macke, R. J. 2008. The Significance of Meteorite Density and Porosity. *Geochemistry* 68: 1–29.

Consolmagno, G. J., Macke, R. J., Rochette, P., Britt, D. T., and Gattacceca, J. 2006. Density, Magnetic Susceptibility, and the Characterization of Ordinary Chondrite Falls and Showers. *Meteoritics & Planetary Science* 41: 331–342.

Dalcher, N., Caffee, M. W., Nishiizumi, K., Welten, K. C., Vogel, N., Wieler, R., and Leya, I. 2013. Calibration of Cosmogenic Noble Gas Production in Ordinary Chondrites Based on ^{36}Cl-^{36}Ar Ages. Part 1: Refined Produced Rates for Cosmogenic ^{21}Ne and ^{38}Ar. *Meteoritics & Planetary Science* 48: 1841–62.

Devillepoix, H. A. R., Cupak, M., Bland, P. A., Sansom, E. K., Towner, M. C., Howie, R. M., Hartig, B. A. D., et al. 2020. A Global Fireball Observatory. *Planetary and Space Science* 191: 105036.

Devillepoix, H. A. R., Sansom, E. K., Bland, P. A., Towner, M. C., Cupák, M., Howie, R. M., Jansen-Sturgeon, T., et al. 2018. The Dingle Dell Meteorite: A Halloween Treat from the Main Belt. *Meteoritics & Planetary Science* 53: 2212–27.

Di Gregorio, M., Busemann, H., Hunt, A. C., Krietsch, D., Schönbächler, M., and Maden, C. 2019. Variable Cosmogenic Argon in L/LL5 Chondrite Knyahinya. *82nd Annual Meeting of the Meteoritical Society*, abstract #2157.

Dunn, T. L., Cressey, G., McSween, H. Y., Jr., and McCoy, T. J. 2010. Analysis of Ordinary Chondrites Using Powder X-Ray Diffraction: 1. Modal Mineral Abundances. *Meteoritics & Planetary Science* 45: 123–134.

Ferus, M., Petera, L., Koukal, J., Lenža, L., Drtinová, B., Haloda, J., Matýsek, D., et al. 2020. Elemental Composition, Mineralogy and Orbital Parameters of the Porangaba Meteorite. *Icarus* 341: 113670.

Ford, R. L., Benedix, G. K., McCoy, T. J., and Rushmer, T. 2008. Partial Melting of H6 Ordinary Chondrite Kernouvé: Constraints on the Effects of Reducing Conditions on Oxidized Compositions. *Meteoritics & Planetary Science* 43: 1399–1414.

Friedrich, J. M., Macke, R. J., Wignarajah, D. P., Rivers, M. L., Britt, D. T., and Ebel, D. S. 2008. Pore Size Distribution in an Uncompacted Equilibrated Ordinary Chondrite. *Planetary and Space Science* 56: 895–900.

Friedrich, J. M., and Rivers, M. L. 2013. Three-Dimensional Imaging of Ordinary Chondrite Microporosity at 2.6 μm Resolution. *Geochimica et Cosmochimica Acta* 116: 63–70.

Friedrich, J. M., Ruzicka, A., Macke, R. J., Thostenson, J. O., Rudolph, R. A., Rivers, M. L., and Ebel, D. S. 2017. Relationships among Physical Properties as Indicators of High Temperature Deformation or Post-Shock Thermal Annealing in Ordinary Chondrites. *Geochimica et Cosmochimica Acta* 203: 157–174.

Friedrich, J. M., Wang, M. S., and Lipschutz, M. E. 2003. Chemical Studies of L Chondrites. V: Compositional Patters for 49 Trace Elements in 14 L4-6 and 7 LL4-6 Falls. *Geochimica et Cosmochimica Acta* 67: 2467–79.

Gardiol, D., Barghini, D., Buzzoni, A., Carbognani, A., Di Carlo, M., Di Martino, M., Knapic, C., et al. 2021. Cavezzo, the First Italian Meteorite Recovered by the PRISMA Fireball Network. Orbit, Trajectory, and Strewn-Field. *Monthly Notices of the Royal Astronomical Society* 501: 1215–27.

Gattacceca, J., Bouvier, A., Grossman, J., Metzler, K., and Uehara, M. 2019. The Meteoritical Bulletin, No. 106. *Meteoritics & Planetary Science* 54: 469–471.

Gattacceca, J., Eisenlohr, P., and Rochette, P. 2004. Calibration of In Situ Magnetic Susceptibility Measurement. *Geophysical Journal International* 158: 42–49.

Glavin, D. P., Callahan, M. P., Dworkin, J. P., and Elsila, J. E. 2010. The Effects of Parent Body Processes on Amino Acids in Carbonaceous Chondrites. *Meteoritics & Planetary Science* 45: 1948–72.

Glavin, D. P., Dworkin, J. P., Aubrey, A., Botta, O., Doty, J. H., III, Martins, Z., and Bada, J. L. 2006. Amino Acid Analyses of Antarctic CM2 Meteorites Using Liquid Chromatography-Time of Flight-Mass Spectrometry. *Meteoritics & Planetary Science* 41: 889–902.

Glavin, D. P., Elsila, J. E., McLain, H. L., Aponte, J. C., Parker, E. T., Dworkin, J. P., Hill, D. H., Connolly, H. C., and Lauretta, D. S. 2021. Extraterrestrial Amino Acids and L-Enantiomeric Excesses in the CM2 Carbonaceous Chondrites Aguas Zarcas and Murchison. *Meteoritics & Planetary Science* 56: 148–173.

Godel, B. 2013. High-Resolution X-Ray Computed Tomography and its Application to Ore Deposits: From Data Acquisition to Quantitative Three-Dimensional Measurements with Case Studies from Ni-Cu-PGE Deposits. *Economic Geology* 108: 2005–19.

Godel, B., Barnes, S. J., and Maier, W. D. 2006. 3-D Distribution of Sulphide Minerals in the Merensky Reef (Bushveld Complex, South Africa) and the JM Reef (Stillwater Complex, USA) and their Relationship to Microstructures Using X-Ray Computed Tomography. *Journal of Petrology* 47: 1853–72.

Goswami, J. N., Lal, D., Rao, M. N., Sinha, N., and Venkatesan, T. R. 1978. Particle Track and Rare Gas Studies of Innisfree Meteorite. *Meteoritical Society, Annual Meeting, 41st, Sudbury, Ontario, Canada, Aug. 14–17, 1978*. *Meteoritics* 13: 481–84.

Granvik, M., and Brown, P. 2018. Identification of Meteorite Source Regions in the Solar System. *Icarus* 311: 271–287.

Halliday, I., Blackwell, A. T., and Griffin, A. A. 1978. The Innisfree Meteorite and the Canadian Camera Network. *Journal of the Royal Astronomical Society of Canada* 72: 15–39.

Howard, K. T., Benedix, G. K., Bland, P. A., and Cressey, G. 2009. Modal Mineralogy of CM2 Chondrites by X-Ray Diffraction (PSD-XRD). Part 1: Total Phyllosilicate Abundance and the Degree of Aqueous Alteration. *Geochimica et Cosmochimica Acta* 73: 4576–89.

Howie, R. M., Paxman, J., Bland, P. A., Towner, M. C., Cupak, M., Sansom, E. K., and Devillepoix, H. A. R. 2017. How to Build a Continental Scale Fireball Camera Network. *Experimental Astronomy* 43: 237–266.

Jarosewich, E. 1990. Chemical Analyses of Meteorites: A Compilation of Stony and Iron Meteorite Analyses. *Meteoritics* 25: 323–337.

Jarosewich, E., Clarke, R. S., Jr., and Barrows, J. N. 1987. Allende Meteorite Reference Sample. *Smithsonian Contributions to the Earth Sciences* 27: 1–49.

Jenniskens, P., and Devillepoix, H. A. 2025. Review of Asteroid, Meteor, and Meteorite-Type Links. *Meteoritics & Planetary Science* 60: 928–973.

Jenniskens, P., Fries, M. D., Yin, Q. Z., Zolensky, M., Krot, A. N., Sanford, S. A., Sears, D., et al. 2012. Radar-Enabled Recovery of the Sutter's Mill Meteorite, a Carbonaceous Chondrite Regolith Breccia. *Science* 338: 1583–87.

Jenniskens, P., Moskovitz, N., Garvie, L. A., Yin, Q. Z., Howell, J. A., Free, D. L., Albers, J., et al. 2020. Orbit and Origin of the LL 7 Chondrite Dishchii'bikoh (Arizona). *Meteoritics & Planetary Science* 55: 535–557.

Jenniskens, P., Rubin, A. E., Yin, Q.-Z., Sears, D. W. G., Sandford, S. A., Zolensky, M. E., Krot, A. N., et al. 2014. Fall, Recovery, and Characterization of the Novato L6 Chondrite Breccia. *Meteoritics & Planetary Science* 49: 1388–1425.

Jenniskens, P., Utas, J., Yin, Q. Z., Matson, R. D., Fries, M., Howell, J. A., Free, D., et al. 2019. The Creston, California, Meteorite Fall and the Origin of L Chondrites. *Meteoritics & Planetary Science* 54: 699–720.

Kalasová, D., Zikmund, T., Spurný, P., Haloda, J., Borovička, J., and Kaiser, J. 2020. Chemical and Physical Properties of Žd'ár Nad Sázavou L Chondrite and Porosity Differentiation Using Computed Tomography. *Meteoritics & Planetary Science* 55: 1073–81.

Kallemeyn, G. W., Rubin, A. E., Wang, D., and Wasson, J. T. 1989. Ordinary Chondrites: Bulk Compositions, Classification, Lithophile-Element Fractionations and Composition-Petrographic Type Relationships. *Geochimica et Cosmochimica Acta* 53: 2747–67.

Keil, K., and Fredriksson, K. 1964. The Iron, Magnesium, and Calcium Distribution in Coexisting Olivines and Rhombic Pyroxenes of Chondrites. *Journal of Geophysical Research* 69: 3487–3515.

Kirby, R. S., King, P. L., and Tomkins, A. G. 2025. A Statistical Investigation into the Relationships between IIE Irons and the Ordinary, F and "HH" Chondrite. *Meteoritics & Planetary Science* 60: 2376–2400.

Korochantseva, E. V., Trieloff, M., Lorenz, C. A., Buykin, A. I., Ivanova, M. A., Schwarz, W. H., Hopp, J., and Jessberger, E. K. 2007. L-Chondrite Asteroid Breakup Tied to Ordovician Meteorite Shower by Multiple Isochron 40Ar-39 Ar Dating. *Meteoritics & Planetary Science* 42: 113–130.

Kővágó, G. 2021. Possible meteorite fall in Austria. *EMeteorNews* 6: 87–89.

Leya, I., and Masarik, J. 2009. Cosmogenic Nuclides in Stony Meteorites Revisited. *Meteoritics & Planetary Science* 44: 1061–86.

Li, S., Yin, Q. Z., Bao, H., Sanborn, M. E., Irving, A., Ziegler, K., Agee, C., et al. 2018. Evidence for a Multilayered Internal Structure of the Chondritic Acapulcoite-Lodranite Parent Asteroid. *Geochimica et Cosmochimica Acta* 242: 82–101.

Llorca, J., Trigo-Rodríguez, J. M., Ortiz, J. L., Docobo, J. A., García-Guinea, J., Castro-Tirado, A. J., Rubin, A. E., et al. 2005. The Villalbeto de la Peña Meteorite Fall: I. Fireball Energy, Meteorite Recovery, Strewn Field, and Petrography. *Meteoritics & Planetary Science* 40: 795–804.

Lodders, K. 2021. Relative Atomic Solar System Abundances, Mass Fractions, and Atomic Masses of the Elements and their Isotopes, Composition of the Solar Photosphere, and

Compositions of the Major Chondritic Meteorite Groups. *Space Science Reviews* 217: 44.

Macke, R. J. 2010. *Survey of Meteorite Physical Properties Density, Porosity and Magnetic Susceptibility*. Doctoral Thesis. Orlando, Florida: University of Central Florida.

Macke, R. J., Benedix, G. K., Bland, P. A., and the D.F.N. Team. 2017. Dingle Dell Density and Other Physical Properties. *80th Annual Meeting of the Meteoritical*, LPI Contribution 1987.

Marsset, M., Vernazza, P., Brož, M., Thomas, C. A., DeMeo, F. E., Burt, B., Binzel, R. P., et al. 2024. The Massalia Asteroid Family as the Origin of Ordinary L Chondrites. *arXiv preprint arXiv:2403.08548*.

Marti, K., and Graf, T. 1992. Cosmic-Ray Exposure History of Ordinary Chondrites. *Annual Review of Earth and Planetary Sciences* 20: 221–243.

Martins, Z., Hofmann, B. A., Gnos, E., Greenwood, R. C., Verchovsky, A., Franchi, I. A., Jull, A. J. T., et al. 2007. Amino Acid Composition, Petrology, Geochemistry, 14C Terrestrial Age and Oxygen Isotopes of the Shişr 033 CR Chondrite. *Meteoritics & Planetary Science* 42: 1581–95.

Meier, M. M., Gritsevich, M., Welten, K. C., Lyytinen, E., Plant, A. A., Maden, C., and Busemann, H. 2020. Orbit, Meteoroid Size and Cosmic History of the Osceola (L6) Meteorite. *European Planetary Science Congress* (EPSC2020-730).

Meier, M. M. M. 2024. Meteoriteorbits.Info—Tracking all Known Meteorites with Photographic Orbits. *Lunar and Planetary Science Conference 2017*, abstract #1178. Accessed 12 July 2024.

Meier, M. M. M., Welten, K. C., Riebe, M. E., Caffee, M. W., Gritsevich, M., Maden, C., and Busemann, H. 2017. Park Forest (L5) and the asteroidal Source of Shocked L Chondrites. *Meteoritics & Planetary Science* 52: 1561–76.

Nesvorný, D., Vokrouhlický, D., Morbidelli, A., and Bottke, W. F. 2009. Asteroidal Source of L Chondrite Meteorites. *Icarus* 200: 698–701.

Nishiizumi, K. 2004. Preparation of ^{26}Al AMS Standards. *Nuclear Instruments and Methods in Physics Research* B223 (224): 388–392.

Nishiizumi, K., Imamura, M., Caffee, M. W., Southon, J. R., Finkel, R. C., and McAninch, J. 2007. Absolute Calibration of ^{10}Be AMS Standards. *Nuclear Instruments and Methods in Physics Research* B258: 403–413.

Nishiizumi, K., Klein, J., Middleton, R., and Craig, H. 1990. Cosmogenic ^{10}Be, ^{26}Al, and ^{3}He in Olivine from Maui Lavas. *Earth and Planetary Science Letters* 98: 263–66.

Oberst, J., Molau, S., Heinlein, D., Gritzner, C., Schindler, M., Spurny, P., Ceplecha, Z., Rendtel, J., and Betlem, H. 1998. The "European Fireball Network": Current Status and Future Prospects. *Meteoritics & Planetary Science* 33: 49–56.

Popova, O. P., Jenniskens, P., Emel'yanenko, V., Kartashova, A., Biryukov, E., Khaibrakhmanov, S., Shuvalov, V., et al. 2013. Chelyabinsk Airburst, Damage Assessment, Meteorite Recovery, and Characterization. *Science* 342: 1069–73.

Pratesi, G., Moggi-Cecchi, V., Greenwood, R. C., Franchi, I. A., Hammond, S. J., Di Martino, M., Barghini, D., Taricco, C., Carbognani, A., and Gardiol, D. 2021. Cavezzo—The Double Face of a Meteorite: Mineralogy, Petrography, and Geochemistry of a Very Unusual Chondrite. *Meteoritics & Planetary Science* 56: 1125–50.

Riebe, M. E. I., Welten, K. C., Meier, M. M. M., Wieler, R., Barth, M. I. F., Ward, D., Laubenstein, M., et al. 2017. Cosmic-Ray Exposure Ages of Six Chondritic Almahata Sitta Fragments. *Meteoritics & Planetary Science* 52: 2353–74.

Righter, K., Abell, P., Agresti, D., Berger, E. L., Burton, A. S., Delaney, J. S., Fries, M. D., et al. 2015. Mineralogy, Petrology, Chronology, and Exposure History of the Chelyabinsk Meteorite and Parent Body. *Meteoritics & Planetary Science* 50: 1790–1819.

Rochette, P., Sagnotti, L., Bourot-Denise, M., Consolmagno, G., Folco, L., Gattacceca, J., Osete, M. L., and Pesonen, L. 2003. Magnetic Classification of Stony Meteorites: 1. Ordinary chondrites. *Meteoritics & Planetary Science* 38: 251–268.

Rubin, A. E. 1990. Kamacite and Olivine in Ordinary Chondrites: Intergroup and Intragroup Relationships. *Geochimica et Cosmochimica Acta* 54: 1217–32.

Rubin, A. E., Kallemeyn, G. W., and Wasson, J. T. 2002. A IAB-Complex Iron Meteorite Containing Low-Ca Clinopyroxene: Northwest Africa 468 and its Relationship to Lodranites and Formation by Impact Melting. *Geochimica et Cosmochimica Acta* 66: 3657–71.

Sanborn, M. E., Wimpenny, J., Williams, C. D., Yamakawa, A., Amelin, Y., Irving, A. J., and Yin, Q. Z. 2019. Carbonaceous Achondrites Northwest Africa 6704/6693: Milestones for Early Solar System Chronology and Genealogy. *Geochimica et Cosmochimica Acta* 245: 577–596.

Scott, E. R., Taylor, G. J., and Keil, K. 1986. Accretion, Metamorphism, and Brecciation of Ordinary Chondrites: Evidence from Petrologic Studies of Meteorites from Roosevelt County, New Mexico. *Journal of Geophysical Research: Solid Earth* 91(B13): E115–E123.

Scott, E. R. D., Greenwood, R. C., Franchi, I. A., and Sanders, I. S. 2009. Oxygen Isotopic Constraints on the Origin and Parent Bodies of Eucrites, Diogenites, and Howardites. *Geochimica et Cosmochimica Acta* 73: 5835–53.

Sharma, P., Bourgeois, M., Elmore, D., Granger, D., Lipschutz, M. E., Ma, X., Miller, T., et al. 2000. PRIME Lab AMS Performance, Upgrades and Research Applications. *Nuclear Instruments and Methods in Physics Research* B172: 112–123.

Sharma, P., Kubik, P. W., Fehn, U., Gove, G. E., Nishiizumi, K., and Elmore, D. 1990. Development of ^{36}Cl Standards for AMS. *Nuclear Instruments and Methods in Physics Research* B52: 410–15.

Sharp, Z. D. 1990. A Laser-Based Microanalytical Method for In Situ Determination of Oxygen Isotope Ratios of Silicates and Oxides. *Geochimica et Cosmochimica Acta* 54: 1353–57.

Shukolyukov, A., and Lugmair, G. W. 2006. The Mn-Cr Isotope Systematics in the Ureilites Kenna and LEW 85440. *Lunar and Planetary Science Conference XXXVII*, abstract #1478.

Simon, S. B., Grossman, L., Clayton, R. N., Mayeda, T. K., Schwade, J. R., Sipiera, P. P., Wacker, J. F., and Wadhwa, M. 2004. The Fall, Recovery, and Classification of the Park Forest Meteorite. *Meteoritics & Planetary Science* 39: 625–634.

Smith, D. G. W. 1980. The Mineral Chemistry of the Innisfree Meteorite. *The Canadian Mineralogist* 18: 433–442.

Spurny, P., Borovicka, J., Haloda, J., Shrbeny, L., and Heinlein, D. 2016. Two Very Precisely Instrumentally Documented Meteorite Falls: Zdar Nad Sazavou and

Stubenberg-Prediction and Reality *79th Annual Meeting of the Meteoritical Society*, Vol. 79, p. 6221.
Spurný, P., Borovička, J., and Shrbený, L. 2006. Automation of the Czech Part of the European Fireball Network: Equipment, Methods and First Results. *Proceedings of the International Astronomical Union* 2(S236): 121–130.
Spurný, P., Borovička, J., and Shrbený, L. 2020. The Žd'ár Nad Sázavou Meteorite Fall: Fireball Trajectory, Photometry, Dynamics, Fragmentation, Orbit, and Meteorite Recovery. *Meteoritics & Planetary Science* 55: 376–401.
Spurný, P., Haloda, J., Borovička, J., Shrbený, L., and Halodová, P. 2014. Reanalysis of the Benešov Bolide and Recovery of Polymict Breccia Meteorites–Old Mystery Solved after 20 Years. *Astronomy & Astrophysics* 570: A39.
Stöffler, D., Hamann, C., and Metzler, K. 2018. Shock Metamorphism of Planetary Silicate Rocks and Sediments: Proposal for an Updated Classification System. *Meteoritics & Planetary Science* 51: 5–49.
Trigo-Rodríguez, J. M., Llorca, J., Castro-Tirado, A. J., Ortiz, J. L., Docobo, J. A., and Fabrega, J. 2006. The Spanish Fireball Network. *Astronomy and Geophysics* 47: 6–26.
Trinquier, A., Birck, J.-L., and Allegre, C. J. 2007. Widespread ^{54}Cr Heterogeneity in the Inner Solar System. *The Astrophysical Journal* 655: 1179–85.
Trinquier, A., Birck, J.-L., Allègre, C. J., Göpel, C., and Ulfbeck, D. 2008. ^{53}Mn–^{53}Cr Systematics of the Early Solar System Revisited. *Geochimica et Cosmochimica Acta* 72: 5146–63.
Ueda, T., Yamashita, K., and Kita, N. 2006. Chromium Isotopic Study of Ureilite. *69th Annual Meteoritical Society Meeting*, abstract #5178.
Vernazza, P., Binzel, R. P., Thomas, C. A., DeMeo, F. E., Bus, S. J., Rivkin, A. S., and Tokunaga, A. T. 2008. Compositional Differences between Meteorites and near-Earth Asteroids. *Nature* 454: 858–860.
Vida, D., Šegon, D., Šegon, M., Atanackov, J., Ambrožič, B., McFadden, L., Ferrière, L., et al. 2021. *Novo Mesto Meteorite Fall–Trajectory, Orbit, and Fragmentation Analysis from Optical Observations*(No. EPSC2021-139). Brussels, Belgium: Copernicus Meetings.
Wasson, J. T., and Kallemeyn, G. W. 1988. Compositions of Chondrites. *Philosophical Transactions of the Royal Society of London. Series A, Mathematical and Physical Sciences* 325: 535–544.
Weirich, J. R., Swindle, T. D., and Isachsen, C. E. 2012. 40Ar-39Ar Age of Northwest Africa 091: More Evidence for a Link between L Chondrites and Fossil Meteorites. *Meteoritics & Planetary Science* 47: 1324–35.
Welten, K. C., Caffee, M. W., Hillegonds, D. J., McCoy, T. J., Masarik, J., and Nishiizumi, K. 2011. Cosmogenic Radionuclides in L5 and LL5 Chondrites from Queen Alexandra Range, Antarctica: Identification of a Large L/LL5 Chondrite Shower with a Preatmospheric Mass of Approximately 50,000 Kg. *Meteoritics & Planetary Science* 46: 177–196.
Wolf, S. F., Compton, J. R., and Gagnon, C. J. 2012. Determination of 11 Major and Minor Elements in Chondritic Meteorites by Inductively Coupled Plasma Mass Spectrometry. *Talanta* 100: 276–281.
Woodcock, N. H. 1977. Specification of Fabric Shapes Using an Eigenvalue Method. *Geological Society of America Bulletin* 88: 1231–36.
Woodcock, N. H., and Naylor, M. 1983. Randomness Testing in Three-Dimensional Orientation Data. *Journal of Structural Geology* 5: 539–548.
Yamakawa, A., Yamashita, K., Makishima, A., and Nakamura, E. 2009. Chemical Separation and Mass Spectrometry of Cr, Fe, Ni, Zn, and Cu in Terrestrial and Extraterrestrial Materials Using Thermal Ionization Mass Spectrometry. *Analytical Chemistry* 81: 9787–94.